Homogenization of thin-structured surfaces for acoustics in the presence of a two-dimensional low Mach potential flow

Jean-François Mercier

Abstract

A surface homogenization method for acoustic waves over thin microstructured surfaces in presence of a fluid in a potential flow is presented. Sound hard surfaces are considered, the flow is considered 2D and slow and a Low Mach approximation is introduced. We consider acoustic waves with a typical wavelength $1/k$ much larger than the array spacing h and thickness e. Owing to the small parameter $\varepsilon = kh$, with $e/h = O(1)$, a matched asymptotic expansion technique is applied to the Low Mach potential wave equation in the frequency domain. A boundary condition is obtained on an equivalent flat wall, which links the acoustic velocity to its normal and tangential derivatives (of the Myers type). The accuracy of the effective model is tested numerically for various periodic shapes and the accuracy of the model in $O(\varepsilon^2)$ is validated.

Homogenization of thin structured surfaces for acoustics in presence of a 2D Low Mach potential flow

Jean-François Mercier[1]

October 12, 2023

1 introduction

We aim at developing an effective model to characterize sound propagation over a periodic acoustically-hard ground. The motivation is due to interesting engineering applications: micro-structured surfaces can absorb acoustic waves. The best known are micro-perforated absorbers and liners for acoustic noise reduction in vehicles or airplanes or for optimal acoustics in conference or lecture halls [1, 2]. For surfaces consisting of rectangular grooves, approximate effective impedance models [3] have been derived and as detailed in [4] roughness can be used to modify effective impedances to enhance the surface transport noise reduction [5, 6]. The key mechanism is the creation of surface waves by roughness near grazing incidence [7]: the energy reaching a receiver can then be reduced by transferring the incident sound energy into these surface waves [8].

When studying ultrasonic waves propagating above a periodic grating, arbitrary grating shapes may be modeled numerically, but frequency-domain or time-domain methods [6, 7] are computationally demanding to properly account for the geometry. For this reason alternative analytical methods are being developed [9, 10, 11, 12], which explicitly determine impedance models, useful for designing grooved surfaces [4, 5]. Closely related to our study, diffraction by an acoustically-hard periodic surface has recently been studied analytically, using two different tools depending on the complexity of the geometry: a modal method [4] for rectangular grooves or a homogenization method for general profiles [13]. In [13], not limited by the geometry, a two-scale homogenization method based on a matched asymptotic expansion technique was used, leading to a boundary condition obtained on an equivalent flat wall. Such surface homogenization and more generally interface homogenizations based on matched asymptotic expansion techniques have been widely used, in acoustics [14, 15, 16, 17] but also in different wave contexts like elastic waves [18] or electromagnetic waves [19, 20, 21, 22].

The purpose of this paper is to extend the acoustic homogenization process presented in [13] from a fluid at rest to a flowing fluid. The primary motivation is

the noise reduction in aircraft engines inlets [23], for which manufacturers apply what is called an acoustic lining along the walls of the inlet duct and bypass duct [24, 25]. The mean flow present in aircraft engines complicates the interaction between the acoustics and the impedance surface and requires modeling tools to be clarified and improved. A common approach is to model the acoustic lining as an Extended Helmholtz Resonator [26]. It consists in considering a porous plate, with small cells underneath, called Helmholtz resonators that induce an impedance by virtue of the air entering through the small hole and oscillating inside the cavity. This leads to the usual boundary conditions for modeling acoustics in flows over acoustic liners [27, 28], namely the Myers condition [29] or the Ingard–Myers condition [30]. These boundary conditions relate the acoustic pressure and the acoustic normal velocity at the lining.

Let us mention that the inclusion of the fluid motion in the homogenization process of [13] is not a simple extension because the mean flow is not a given data: it must also be determined since it depends on the geometry, using a homogenization process, and moreover the acoustics is coupled to the flow which implies that the two quantities must be determined jointly. The consequence is that two coupled homogenized problems will be determined in parallel, for the mean flow and for the acoustic waves. Because of this complexity, we will not homogenize the most general case described by the compressible Navier-Stokes equations but on the contrary we will manipulate a less general model which is better adapted to a homogenization process: we restrict to a curl-free mean flow (then the acoustics perturbations are also naturally curl-free) and we neglect the viscosity. To assume curl-free quantities has two huge advantages: the flow is easy to determine while taking into account the geometry of the wavy surface and for the acoustic perturbations, the starting equations are simple enough to lead to an easy-to-handle homogenized model.

Let us also mention that such homogenization process applied to acoustic reflection in a moving fluid on a non-planar surface has not been performed before, but there are some related studies on flow-coupled acoustics in the context of the homogenization. The problem of acoustic waves influenced by the advection velocity field has been treated in a bulk porous rigid and in deformable media [31], or in a layer containing a perforated plate [32], with particular examples using a potential flow model. Moreover the transfer of incident waves into surface waves has been discussed in [33] and [34], characterizing in particular the influence of the shape of the plate perforations. But apart from these works, it is mainly the study of the flow alone that has been considered but in another context and with other equations: this has been done for lubrication applications, with the determination of the effective boundary conditions for a viscous flow on a periodic surface. Then, the viscosity is introduced, the stationary Navier-Stokes equations are solved and the homogeneous Dirichlet boundary conditions are considered instead of the usual Neumann conditions in acoustics. Most of the time, the case of an incompressible fluid has been considered [35, 36, 37, 38, 39, 40, 41, 42, 43]. The compressible case, closer to acoustic applications we are interested in, has been less studied [44, 45, 46]. However, these studies, designed for hydrodynamic phenomena, do not apply

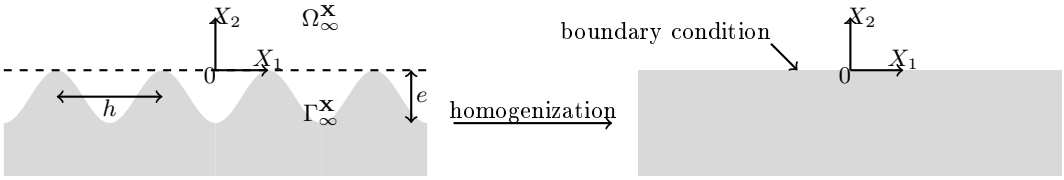

Figure 1: Left: surface structured with periodic rigid roughnesses; Right: the homogenization gives a boundary condition to apply on a flat surface.

to our acoustic configuration because of two specificities: they include viscosity, which plays an important role whereas it is neglected in acoustics, and they consider isothermal transformations, which are not adapted to the development of acoustic waves.

The paper is organized as follows. Section 2 presents the different models available to describe acoustic propagation in a flow and focuses in particular on a Low Mach flow (the derivations of the different models, exact or approximated, are detailed in the appendix). Section 3 details the derivation of the homogenized model. Finally, section 4 is devoted to some numerical results, highlighting the efficiency and testing the accuracy of the homogenized model.

2 Equations for the low Mach acoustic propagation in a potential flow

2.1 General equations

Acoustic propagation without flow is governed by the simple scalar Helmholtz equation. Adding a motion of the fluid induces additional difficulties leading to complex models. The propagation in a general mean flow requires to use vectorial equations: Linearized Euler's Equation, Galbrun's equations [47, 48], Möhring equations [49, 50] or Goldstein's equation [51]. A popular and simpler approach that we will follow is to consider an adiabatic irrotational mean flow. Then the linear equations satisfied by the acoustic perturbations reduce [52, 53, 54] to a scalar wave equation (3) that we will call the potential wave equation as in [55]. But even this potential case reveals complicated in practice and various transformations are traditionally used to simplify this equation. For a uniform mean flow, the potential wave equation, then called the uniform flow Helmholtz equation [56], is reduced to the standard Helmholtz problem without approximations thanks to the Lorentz transformation [57, 58]. For representing non-uniform mean flow effects, approximate formulations for wave propagation have been derived [59, 60, 61] in the case of low Mach numbers mean flows and it is the approach we will follow.

Let us introduce some notations to precise the model that will be homogenized. A 2D domain $\Omega_\infty^{\mathbf{X}}$ bounded by a rigid boundary $\Gamma_\infty^{\mathbf{X}}$ with $\mathbf{X} = (X_1, X_2)$

the coordinates in the physical space (see Fig. 1) is considered. To simplify we suppose that the boundary $\Gamma_\infty^{\mathbf{X}}$ is given by a function f such that $X_2 = hf(X_1/h)$ with f a 1-periodic piecewise C^1 function. Therefore we have the definitions $\Gamma_\infty^{\mathbf{X}} = \{(X_1, X_2) \in \mathbb{R}^2; X_2 = hf(X_1/h)\}$ and $\Omega_\infty^{\mathbf{X}} = \{(X_1, X_2) \in \mathbb{R}^2; X_2 > hf(X_1/h)\}$. For a more complicated boundary shape like a polygonal wall, a parametric description $(X_1(s), X_2(s))$, $s \in [0,1]$, of the surface should be introduced with X_1 and X_2 chosen as piecewise C^1 functions. We consider an adiabatic potential mean flow of uniform velocity $\boldsymbol{U}_\infty$ at infinity, of modulus noted $|\boldsymbol{U}_\infty| = U_\infty$. This irrotational flow satisfying compressible Euler's equations is sought in the form $U_\infty \boldsymbol{U}$ with $\boldsymbol{U}(\mathbf{X})$ of modulus unitary at infinity, associated to the potential $\Phi(\mathbf{X})$ such that $\boldsymbol{U} = \boldsymbol{\nabla}_{\mathbf{X}}\Phi$. The mean flow satisfies (see Appendix A.1)

$$\left\{\begin{array}{rcll} \mathrm{div}_{\mathbf{X}}\left(\rho_0 \boldsymbol{U}\right) & = & 0 & \text{in } \Omega_\infty^{\mathbf{X}}, \\ \boldsymbol{U} & = & \boldsymbol{\nabla}_{\mathbf{X}}\Phi & \text{in } \Omega_\infty^{\mathbf{X}}, \\ \boldsymbol{U}\cdot\boldsymbol{n} & = & 0 & \text{on } \Gamma_\infty^{\mathbf{X}}, \\ \lim_{X_2\to\infty} \boldsymbol{U} & = & \boldsymbol{U}_\infty/U_\infty. & \end{array}\right. \tag{1}$$

The equations are non-linear since the coefficients depend on the velocity: the dimensionless sound speed c_0 and the the dimensionless density ρ_0 are given for an adiabatic flow of adiabatic index γ by

$$c_0^2 = 1 + \frac{\gamma-1}{2} M^2 (1 - |\boldsymbol{U}|^2) = \rho_0^{\gamma-1}. \tag{2}$$

For the acoustic perturbations, we consider the time harmonic regime of frequency ω ($e^{-i\omega t}$ dependence). We define the Mach number at infinity $M = U_\infty/c_\infty$ where c_∞ is the sound velocity at infinity. The acoustic perturbations are associated to a velocity potential $\varphi(\mathbf{X})$ satisfying the potential wave equation [55]

$$\left\{\begin{array}{rcll} \rho_0 \mathrm{D}_{\mathbf{X}}\left(\frac{1}{c_0^2}\mathrm{D}_{\mathbf{X}}\varphi\right) & = & \mathrm{div}_{\mathbf{X}}\left(\rho_0 \boldsymbol{\nabla}_{\mathbf{X}}\varphi\right) & \text{in } \Omega_\infty^{\mathbf{X}}, \\ \boldsymbol{\nabla}_{\mathbf{X}}\varphi\cdot\boldsymbol{n} & = & 0 & \text{on } \Gamma_\infty^{\mathbf{X}}, \end{array}\right. \tag{3}$$

where the convective operator is defined by $\mathrm{D}_{\mathbf{X}} = M\boldsymbol{U}\cdot\boldsymbol{\nabla}_{\mathbf{X}} - ik$, with $k = \omega/c_\infty$ the acoustic wave number. The derivation of these equations (1), (2), (3) is detailed in the Appendix A.2. These equations have the advantage to be exact but their non-linearity makes homogenization difficult to perform. However the equations simplify in a convenient way better suited to homogenization when considering a slow flow as detailed in the next paragraph and we will consider this Low Mach model in the rest of the paper.

2.2 Low Mach model

To consider a low Mach number is a classic approach [37, 55, 60, 62, 63, 64, 65, 66, 67]. Neglecting the terms of order M^2, the potential wave equation becomes the Taylor wave equation (4) as named in [55]:

$$\left\{\begin{array}{rcll} \Delta_{\mathbf{X}}\varphi + k^2\varphi + 2ikM\boldsymbol{U}\cdot\boldsymbol{\nabla}_{\mathbf{X}}\varphi &=& 0 & \text{in } \Omega_\infty^{\mathbf{X}}, \\ \boldsymbol{\nabla}_{\mathbf{X}}\varphi\cdot\boldsymbol{n} &=& 0 & \text{on } \Gamma_\infty^{\mathbf{X}}, \end{array}\right. \tag{4}$$

whereas the mean flow satisfies the simplified equations, now linear

$$\left\{\begin{array}{rcll} \mathrm{div}_{\mathbf{X}}\,\boldsymbol{U} &=& 0 & \text{in } \Omega_\infty^{\mathbf{X}}, \\ \boldsymbol{U} &=& \boldsymbol{\nabla}_{\mathbf{X}}\Phi & \text{in } \Omega_\infty^{\mathbf{X}}, \\ \boldsymbol{U}\cdot\boldsymbol{n} &=& 0 & \text{on } \Gamma_\infty^{\mathbf{X}}, \\ \lim_{X_2\to\infty}\boldsymbol{U} &=& \boldsymbol{U}_\infty/U_\infty. & \end{array}\right. \tag{5}$$

This Low Mach model is derived in the Appendix B. Note that these equations can be written with only the potentials (φ, Φ):

$$\left\{\begin{array}{rcll} \Delta_{\mathbf{X}}\varphi + k^2\varphi + 2ikM\boldsymbol{\nabla}_{\mathbf{X}}\Phi\cdot\boldsymbol{\nabla}_{\mathbf{X}}\varphi &=& 0 & \text{in } \Omega_\infty^{\mathbf{X}}, \\ \boldsymbol{\nabla}_{\mathbf{X}}\varphi\cdot\boldsymbol{n} &=& 0 & \text{on } \Gamma_\infty^{\mathbf{X}}, \\ \Delta_{\mathbf{X}}\Phi &=& 0 & \text{in } \Omega_\infty^{\mathbf{X}}, \\ \boldsymbol{\nabla}_{\mathbf{X}}\Phi\cdot\boldsymbol{n} &=& 0 & \text{on } \Gamma_\infty^{\mathbf{X}}, \\ \lim_{X_2\to\infty}\boldsymbol{\nabla}_{\mathbf{X}}\Phi &=& \boldsymbol{U}_\infty/U_\infty. & \end{array}\right. \tag{6}$$

Notably with this formulation, it is clear that Φ satisfies the equations for φ with $k = 0 = M$.

2.3 Scaled equations

The homogenization will be done on dimensionless equations. Introducing the dimensionless coordinates $\mathbf{x} = k\mathbf{X}$ and introducing the changes of unknowns $\varphi(\mathbf{x}) = \varphi(\mathbf{X})$ (we should introduce an extra notation of the type $\tilde{\varphi}(\mathbf{x}) = \varphi(\mathbf{X})$, but we prefer to keep simple notations), $\boldsymbol{U}(\mathbf{x}) = \boldsymbol{U}(\mathbf{X})$ and the velocity potential $\Phi(\mathbf{x}) = k\Phi(\mathbf{X})$, we get the coupled system for $(\varphi, \boldsymbol{U}, \Phi)$ in the $\mathbf{x} = (x_1, x_2)$ space:

$$\left\{\begin{array}{rcll} \Delta_{\mathbf{x}}\varphi + \varphi + 2iM\boldsymbol{U}\cdot\boldsymbol{\nabla}_{\mathbf{x}}\varphi &=& 0 & \text{in } \Omega_\infty, \\ \boldsymbol{\nabla}_{\mathbf{x}}\varphi\cdot\boldsymbol{n} &=& 0 & \text{on } \Gamma_\infty, \\ \mathrm{div}_{\mathbf{x}}\,\boldsymbol{U} &=& 0 & \text{in } \Omega_\infty, \\ \boldsymbol{U} &=& \boldsymbol{\nabla}_{\mathbf{x}}\Phi & \text{in } \Omega_\infty, \\ \boldsymbol{U}\cdot\boldsymbol{n} &=& 0 & \text{on } \Gamma_\infty, \\ \lim_{X_2\to\infty}\boldsymbol{U} &=& \boldsymbol{U}_\infty/U_\infty, & \end{array}\right. \tag{7}$$

where Ω_∞ and Γ_∞ are $\Omega_\infty^{\mathbf{X}}$ and $\Gamma_\infty^{\mathbf{X}}$ expressed in the $\boldsymbol{x}$ coordinates (see Fig. 2).

Now we restrict to a periodic geometry with a surface Γ_∞ of period noted h and of vertical extent e both supposed small in front of the wavelength $\lambda = 2\pi/k$, and we homogenize the Low Mach model (7).

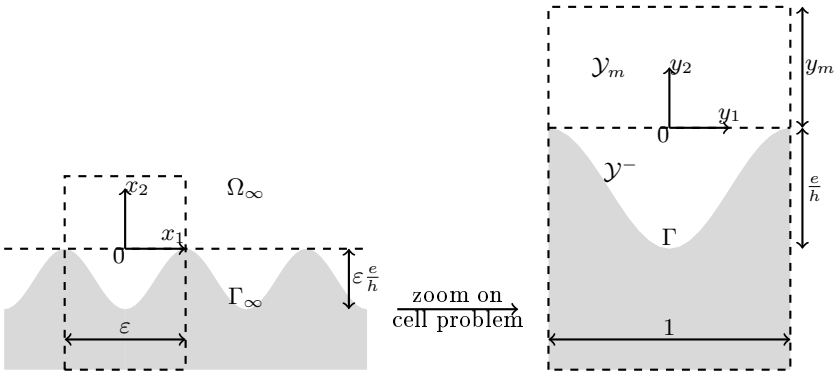

Figure 2: The surface structured by periodic roughnesses in the two coordinates systems $\mathbf{x}$ and $\mathbf{y} = \mathbf{x}/\varepsilon$. In the $\mathbf{y}$-coordinates, the regions occupied by the fluid are noted $\mathcal{Y}_m$ for $f(y_1) < y_2 < y_m$, $\mathcal{Y}^-$ for $y_m = 0$ and $\mathcal{Y} = \lim_{y_m \to \infty} \mathcal{Y}_m$. Γ is the lower boundary of $\mathcal{Y}_m$ at $y_2 = f(y_1)$ associated to a homogeneous Neumann boundary condition.

3 Homogenized model for the diffraction by a periodic surface

3.1 Geometry and main result

The period h of $\Gamma_\infty^{\mathbf{X}}$ becomes $\varepsilon = kh$ for Γ_∞ (see Fig. 2) and the boundary is defined by $\Gamma_\infty = \{(x_1, x_2) \in \mathbb{R}^2; x_2 = \varepsilon f(x_1/\varepsilon)\}$. For convenience the origin $x_2 = 0$ is chosen such that $f \leq 0$ and the effective boundary condition will be determined at $x_2 = 0$. We note $e = h \sup_{y_1 \in [0,1]} |f(y_1)|$ the maximum depth of the periodic surface and we suppose that $e/h = O(1)$ which corresponds to a thin surface. The 2D acoustic propagation domain is $\Omega_\infty = \{(x_1, x_2) \in \mathbb{R}^2; x_2 > \varepsilon f(x_1/\varepsilon)\}$.

In this section (3) we will prove the main result of the paper that we present now and that we write with dimensional variables as it will be used in the numerical section.

Homogenized problem:

The unknowns (φ, Φ) of the Low Mach model ((4), (5)) can be approximated at the order 2 (in the sense that the error is of the order of $(kh)^2$) by the unknowns (φ^h, Φ^h) solutions of the following homogenized model, made of the acoustic part

$$\left\{ \begin{array}{rcl} \left(\Delta_{\mathbf{X}} + k^2 + 2ikM\boldsymbol{\nabla}_{\mathbf{X}}\Phi^h \cdot \boldsymbol{\nabla}_{\mathbf{X}}\right)\varphi^h = 0, & \text{for} & X_2 > 0, \\ \dfrac{\partial \varphi^h}{\partial X_2} + hC\left(\dfrac{\partial^2 \varphi^h}{\partial X_1^2} + 2ikM\dfrac{\partial \Phi^h}{\partial X_1}\dfrac{\partial \varphi^h}{\partial X_1}\right) + k^2 hS\varphi^h = 0, & \text{at} & X_2 = 0, \end{array} \right. \tag{8}$$

coupled to the equations for the mean flow

$$\left\{\begin{array}{rl} \Delta_{\mathbf{X}}\Phi^h = 0, & \text{for} \quad X_2 > 0, \\ \dfrac{\partial \Phi^h}{\partial X_2} + hC\dfrac{\partial^2 \Phi^h}{\partial X_1^2} = 0 & \text{at} \quad X_2 = 0, \\ \lim_{X_2\to\infty} \boldsymbol{\nabla}_{\mathbf{X}}\Phi^h = \boldsymbol{U}_\infty/U_\infty. & \end{array}\right. \tag{9}$$

The constants C and S depend only on the shape of the surface Γ_∞ and will be defined later in (20) and (23). Of course if $M = 0$ in (8) we recover the same model than in [13] studying the fluid at rest case (equation (9) cannot exist in [13]). Note that (8) and (9) can be written in a form closer to ((4), (5)), introducing the homogenized flow velocity $\boldsymbol{U}^h = \boldsymbol{\nabla}_{\mathbf{X}}\Phi^h$:

$$\left\{\begin{array}{rll} \left(\Delta_{\mathbf{X}} + k^2 + 2ikM\boldsymbol{U}^h\cdot\boldsymbol{\nabla}_{\mathbf{X}}\right)\varphi^h = 0, & \text{for} & X_2 > 0, \\ \dfrac{\partial \varphi^h}{\partial X_2} + hC\left(\dfrac{\partial^2\varphi^h}{\partial X_1^2} + 2ikM(\boldsymbol{U}^h)_1\dfrac{\partial\varphi^h}{\partial X_1}\right) + k^2hS\varphi^h = 0, & \text{at} & X_2 = 0, \\ \operatorname{div}_{\mathbf{X}}\boldsymbol{U}^h = 0, & \text{for} & X_2 > 0, \\ \boldsymbol{U}^h = \boldsymbol{\nabla}_{\mathbf{x}}\Phi^h, & \text{for} & X_2 > 0, \\ (\boldsymbol{U}^h)_2 + hC\dfrac{\partial(\boldsymbol{U}^h)_1}{\partial X_1} = 0 & \text{at} & X_2 = 0, \end{array}\right.$$

where $(\boldsymbol{U}^h)_i$ designs the i^{th} component of $\boldsymbol{U}^h$.

Remark 1. *With this writing is recognized that the boundary condition for the mean flow is the Beavers and Joseph's law, although this latter is derived in another context: for the flat interface between a porous medium and a laminar flow [35, 39].*

The rest of this section (3) is devoted to the derivation of (8) and of (9). The approach is very close to the procedure presented in [13]. Calculations are easier to perform with dimensionless equations as presented now.

3.2 Derivation of the iterative homogenized models

Introducing $\boldsymbol{u}$ as an extra unknown (it can be interpreted as the acoustic velocity), the equations (7) are written as first order equations,

$$\left\{\begin{array}{rcll} \boldsymbol{u} & = & \boldsymbol{\nabla}_{\mathbf{x}}\varphi & \text{in} \quad \Omega_\infty, \\ \operatorname{div}_{\mathbf{x}}\boldsymbol{u} & = & -\varphi - 2iM\boldsymbol{U}\cdot\boldsymbol{\nabla}_{\mathbf{x}}\varphi & \text{in} \quad \Omega_\infty, \\ \boldsymbol{u}\cdot\boldsymbol{n} & = & 0 & \text{on} \quad \Gamma_\infty, \end{array}\right.$$

for the acoustics, associated to the equations

$$\left\{\begin{array}{rcll} \boldsymbol{U} & = & \boldsymbol{\nabla}_{\mathbf{x}}\Phi & \text{in} \quad \Omega_\infty, \\ \operatorname{div}_{\mathbf{x}}\boldsymbol{U} & = & 0 & \text{in} \quad \Omega_\infty, \\ \boldsymbol{U}\cdot\boldsymbol{n} & = & 0 & \text{on} \quad \Gamma_\infty, \end{array}\right.$$

for the mean flow. Note that the equations for the flow are not obtained simply by taking $k = 0 = M$ in the equations for the acoustics since k has disappeared in the scaling process.

Remark 2. *For the acoustics, since* $\boldsymbol{u} = \boldsymbol{\nabla}_{\mathbf{x}}\varphi$, *instead of* $\operatorname{div}_{\mathbf{x}} \boldsymbol{u} = -\varphi - 2iM\boldsymbol{U}\cdot\boldsymbol{\nabla}_{\mathbf{x}}\varphi$, *we could write* $\operatorname{div}_{\mathbf{x}} \boldsymbol{u} = -\varphi - 2iM\boldsymbol{U}\cdot\boldsymbol{u}$. *We have checked that as expected, it leads to the same homogenized model, the calculations are just slightly less convenient. Since* $\operatorname{div}_{\mathbf{x}} \boldsymbol{U} = 0$ *we could also use the compact and thus elegant writing* $\operatorname{div}_{\mathbf{x}}(\boldsymbol{u} + 2iM\boldsymbol{U}\varphi) = -\varphi$ *but here also calculations turn out to be less convenient.*

Now we introduce asymptotic expansions of the unknowns, which are different according to the distance from the rigid surface.

3.2.1 Outer problem

In the outer region, far from the rigid surface, the unknowns are sought as the following expansions

$$\left\{\begin{array}{rcl} \boldsymbol{u}(x_1,x_2) & = & \boldsymbol{u}^0(x_1,x_2) + \varepsilon\boldsymbol{u}^1(x_1,x_2) + \cdots, \\ \varphi(x_1,x_2) & = & \varphi^0(x_1,x_2) + \varepsilon\varphi^1(x_1,x_2) + \cdots, \end{array}\right.$$

and

$$\left\{\begin{array}{rcl} \boldsymbol{U}(x_1,x_2) & = & \boldsymbol{U}^0(x_1,x_2) + \varepsilon\boldsymbol{U}^1(x_1,x_2) + \cdots, \\ \Phi(x_1,x_2) & = & \Phi^0(x_1,x_2) + \varepsilon\Phi^1(x_1,x_2) + \cdots. \end{array}\right.$$

At order zero we get

$$\left\{\begin{array}{rcl} \boldsymbol{u}^0 & = & \boldsymbol{\nabla}_{\mathbf{x}}\varphi^0, \\ \operatorname{div}_{\mathbf{x}} \boldsymbol{u}^0 & = & -\varphi^0 - 2iM\boldsymbol{U}^0\cdot\boldsymbol{\nabla}_{\mathbf{x}}\varphi^0, \end{array}\right.$$

combined to

$$\left\{\begin{array}{rcl} \boldsymbol{U}^0 & = & \boldsymbol{\nabla}_{\mathbf{x}}\Phi^0, \\ \operatorname{div}_{\mathbf{x}} \boldsymbol{U}^0 & = & 0. \end{array}\right.$$

Therefore we get the volume equations

$$\left\{\begin{array}{rcl} \left(\Delta_{\mathbf{x}} + 1 + 2iM\boldsymbol{U}^0\cdot\boldsymbol{\nabla}_{\mathbf{x}}\right)\varphi^0 & = & 0, \\ \Delta_{\mathbf{x}}\Phi^0 & = & 0, \end{array}\right.$$

associated to $\boldsymbol{u}^0 = \boldsymbol{\nabla}_{\mathbf{x}}\varphi^0$ and $\boldsymbol{U}^0 = \boldsymbol{\nabla}_{\mathbf{x}}\Phi^0$.

At order one we simply get

$$\left\{\begin{array}{rcl} \left(\Delta_{\mathbf{x}} + 1 + 2iM\boldsymbol{U}^0\cdot\boldsymbol{\nabla}_{\mathbf{x}}\right)\varphi^1 + 2iM\boldsymbol{U}^1\cdot\boldsymbol{\nabla}_{\mathbf{x}}\varphi^0 & = & 0, \\ \Delta_{\mathbf{x}}\Phi^1 & = & 0, \end{array}\right.$$

with $\boldsymbol{u}^1 = \boldsymbol{\nabla}_{\mathbf{x}}\varphi^1$ and $\boldsymbol{U}^1 = \boldsymbol{\nabla}_{\mathbf{x}}\Phi^1$.

Now we will derive boundary conditions for $\boldsymbol{u}^0$, $\boldsymbol{U}^0$, $\boldsymbol{u}^1$ and $\boldsymbol{U}^1$.

3.2.2 Inner problem

Close to the boundary Γ_∞, we choose to look for solutions as expansions of the form

$$\left\{\begin{array}{rcl} \boldsymbol{u}(x_1,x_2) & = & \boldsymbol{v}^0(x_1,y_1,y_2)+\varepsilon\boldsymbol{v}^1(x_1,y_1,y_2)+\cdots, \\ \varphi(x_1,x_2) & = & \psi^0(x_1,y_1,y_2)+\varepsilon\psi^1(x_1,y_1,y_2)+\cdots, \\ \boldsymbol{U}(x_1,x_2) & = & \boldsymbol{V}^0(x_1,y_1,y_2)+\varepsilon\boldsymbol{V}^1(x_1,y_1,y_2)+\cdots, \\ \Phi(x_1,x_2) & = & \Psi^0(x_1,y_1,y_2)+\varepsilon\Psi^1(x_1,y_1,y_2)+\cdots, \end{array}\right. \tag{10}$$

where $\mathbf{y}$ are the fast variables, defined by $\mathbf{x}=\varepsilon\mathbf{y}$ and for $n\geq 0$, $\boldsymbol{v}^n(x_1,y_1,y_2)$, $\psi^n(x_1,y_1,y_2)$, $\boldsymbol{V}^n(x_1,y_1,y_2)$ and $\Psi^n(x_1,y_1,y_2)$ are chosen as 1-periodic functions with respect to y_1. The expansions (10) with the two scales $\mathbf{x}$ and $\mathbf{y}$ correspond to the following changes of operators

$$\left\{\begin{array}{rcl} \boldsymbol{\nabla}_{\mathbf{x}} & \to & \dfrac{1}{\varepsilon}\boldsymbol{\nabla}_{\mathbf{y}}+\boldsymbol{e}_1\dfrac{\partial}{\partial x_1}, \\ \mathrm{div}_{\mathbf{x}} & \to & \dfrac{1}{\varepsilon}\,\mathrm{div}_{\mathbf{y}}+\dfrac{\partial}{\partial x_1}\left(\boldsymbol{e}_1\cdot\right), \\ \boldsymbol{U}\cdot\boldsymbol{\nabla}_{\mathbf{x}} & \to & \dfrac{1}{\varepsilon}\boldsymbol{U}\cdot\boldsymbol{\nabla}_{\mathbf{y}}+(\boldsymbol{U})_1\dfrac{\partial}{\partial x_1}, \end{array}\right.$$

with $(\boldsymbol{e}_1,\boldsymbol{e}_2)$ the vector basis of $\mathbb{R}^2$ and $(\boldsymbol{U})_1=\boldsymbol{U}\cdot\boldsymbol{e}_1$.

In the $\mathbf{y}$ coordinates, the rigid boundary becomes located at $y_2=f(y_1)$. Thanks to the y_1-periodicity, we can restrict the resolution to a periodic cell $\mathcal{Y}=\{\mathbf{y}\in(-1/2,1/2)\times\mathbb{R}, y_2>f(y_1)\}$ of rigid lower boundary $\Gamma=\{\mathbf{y}\in(-1/2,1/2)\times\mathbb{R}, y_2=f(y_1)\}$ (see Fig. 2).

• **Order** 0

At order 0, $(\boldsymbol{v}^0,\psi^0,\boldsymbol{V}^0,\Psi^0)$ satisfy the acoustic equations

$$\left\{\begin{array}{rcll} \boldsymbol{\nabla}_{\mathbf{y}}\psi^0 & = & 0 & \text{in } \mathcal{Y}, \\ \mathrm{div}_{\mathbf{y}}\,\boldsymbol{v}^0 & = & -2iM\boldsymbol{V}^0\cdot\boldsymbol{\nabla}_{\mathbf{y}}\psi^0 & \text{in } \mathcal{Y}, \\ \boldsymbol{v}^0\cdot\boldsymbol{n} & = & 0 & \text{on } \Gamma, \end{array}\right. \tag{11}$$

combined to the mean flow equations

$$\left\{\begin{array}{rcll} \boldsymbol{\nabla}_{\mathbf{y}}\Psi^0 & = & 0 & \text{in } \mathcal{Y}, \\ \mathrm{div}_{\mathbf{y}}\,\boldsymbol{V}^0 & = & 0 & \text{in } \mathcal{Y}, \\ \boldsymbol{V}^0\cdot\boldsymbol{n} & = & 0 & \text{on } \Gamma. \end{array}\right. \tag{12}$$

The matching conditions at order 0 are

$$\left\{\begin{array}{rcl} \lim\limits_{y_2\to\infty}\psi^0(x_1,y_1,y_2) & = & \varphi^0(x_1,0), \\ \lim\limits_{y_2\to\infty}\boldsymbol{v}^0(x_1,y_1,y_2) & = & \boldsymbol{u}^0(x_1,0), \end{array}\right.$$

for the acoustics and

$$\left\{\begin{array}{rcl} \lim\limits_{y_2\to\infty}\Psi^0(x_1,y_1,y_2) & = & \Phi^0(x_1,0), \\ \lim\limits_{y_2\to\infty}\boldsymbol{V}^0(x_1,y_1,y_2) & = & \boldsymbol{U}^0(x_1,0), \end{array}\right.$$

for the mean flow. From (11) is deduced that $\psi^0(x_1,y_1,y_2)=\psi^0(x_1)$, implying that $\varphi^0(x_1,0)=\psi^0(x_1)$ from the matching conditions and that $\mathrm{div}_{\mathbf{y}}\,\boldsymbol{v}^0=0$. Integrating $\mathrm{div}_{\mathbf{y}}\,\boldsymbol{v}^0=0$ over the bounded volume $\mathcal{Y}_m$ defined for any $y_m>0$ by $\mathcal{Y}_m=\{\mathbf{y}\in\mathcal{Y}, y_2<y_m\}$ (see Fig. 2), combined with the boundary condition $\boldsymbol{v}^0\cdot\boldsymbol{n}=0$ on Γ and the periodic boundary conditions between $y_1=-1/2$ and $y_1=1/2$, it gives

$$\int_{-1/2}^{1/2}(\boldsymbol{v}^0)_2(x_1,y_1,y_m)\,dy_1=0 \ \text{ for all } \ y_m>0 \ \text{ and thus } \ \lim_{y_2\to\infty}\int_{-1/2}^{1/2}(\boldsymbol{v}^0)_2(x_1,y_1,y_2)\,dy_1=0.$$

Since the 0-order matching conditions give

$$\lim_{y_2\to\infty}\int_{-1/2}^{1/2}(\boldsymbol{v}^0)_2(x_1,y_1,y_2)\,dy_1=\int_{-1/2}^{1/2}(\boldsymbol{u}^0)_2(x_1,0)\,dy_1=(\boldsymbol{u}^0)_2(x_1,0),$$

we deduce the complete boundary conditions for $\boldsymbol{u}^0=(\boldsymbol{u}^0)_1\boldsymbol{e}_1+(\boldsymbol{u}^0)_2\boldsymbol{e}_2$

$$\left\{\begin{array}{rcl}(\boldsymbol{u}^0)_2(x_1,0) &=& 0,\\ (\boldsymbol{u}^0)_1(x_1,0) &=& \dfrac{\partial\varphi^0}{\partial x_1}(x_1,0)=\dfrac{d\psi^0}{dx_1},\end{array}\right. \tag{13}$$

where we have used $\boldsymbol{u}^0=\boldsymbol{\nabla}_{\mathbf{x}}\varphi^0$. Proceeding in a same way from (12) is deduced that $\Psi^0(x_1,y_1,y_2)=\Psi^0(x_1)=\Phi^0(x_1,0)$ and the 0-order matching conditions give

$$\left\{\begin{array}{rcl}(\boldsymbol{U}^0)_2(x_1,0) &=& 0,\\ (\boldsymbol{U}^0)_1(x_1,0) &=& \dfrac{\partial\Phi^0}{\partial x_1}(x_1,0)=\dfrac{d\Psi^0}{dx_1}.\end{array}\right. \tag{14}$$

Therefore at order 0 the surface is seen flat, located at $x_2=0$ and is hard with vanishing normal velocities, for the mean flow and for the acoustics.

• **Order** 1

Now we determine the next order, in particular $\boldsymbol{v}^1$ and ψ^1. At order 1 $(\boldsymbol{v}^1,\psi^1,\boldsymbol{V}^1,\Psi^1)$ satisfy

$$\left\{\begin{array}{rcll}\boldsymbol{v}^0 &=& \boldsymbol{\nabla}_{\mathbf{y}}\psi^1+\boldsymbol{e}_1\dfrac{\partial\psi^0}{\partial x_1} & \text{in } \mathcal{Y},\\ \mathrm{div}_{\mathbf{y}}\,\boldsymbol{v}^1+\dfrac{\partial(\boldsymbol{v}^0)_1}{\partial x_1} &=& -\psi^0 & \\ & & -2iM\left(\boldsymbol{V}^0\cdot\boldsymbol{\nabla}_{\mathbf{y}}\psi^1+(\boldsymbol{V}^0)_1\dfrac{d\psi^0}{dx_1}\right) & \text{in } \mathcal{Y},\\ \boldsymbol{v}^1\cdot\boldsymbol{n} &=& 0 & \text{on } \Gamma,\end{array}\right.$$

combined to

$$\left\{\begin{array}{rcll}\boldsymbol{V}^0 &=& \boldsymbol{\nabla}_{\mathbf{y}}\Psi^1+\boldsymbol{e}_1\dfrac{\partial\Psi^0}{\partial x_1} & \text{in } \mathcal{Y},\\ \mathrm{div}_{\mathbf{y}}\,\boldsymbol{V}^1+\dfrac{\partial(\boldsymbol{V}^0)_1}{\partial x_1} &=& 0 & \text{in } \mathcal{Y},\\ \boldsymbol{V}^1\cdot\boldsymbol{n} &=& 0 & \text{on } \Gamma.\end{array}\right.$$

We start by determining ψ^1. Collecting all the equations describing $\boldsymbol{v}^0$

$$\left\{\begin{array}{rcll} \mathrm{div}_{\mathbf{y}}\,\boldsymbol{v}^0 &=& 0 & \text{in } \mathcal{Y},\\ \boldsymbol{v}^0 &=& \boldsymbol{\nabla}_{\mathbf{y}}\psi^1 + \boldsymbol{e}_1\dfrac{d\psi^0}{dx_1} & \text{in } \mathcal{Y},\\ \boldsymbol{v}^0\cdot\boldsymbol{n} &=& 0 & \text{on } \Gamma, \end{array}\right.$$

is deduced the following problem: ψ^1 is 1-periodic with respect to y_1 and satisfies

$$\left\{\begin{array}{rcll} \Delta_{\mathbf{y}}\psi^1 &=& 0 & \text{in } \mathcal{Y},\\ \boldsymbol{\nabla}_{\mathbf{y}}\psi^1\cdot\boldsymbol{n} &=& -(\boldsymbol{e}_1\cdot\boldsymbol{n})\dfrac{d\psi^0}{dx_1} & \text{on } \Gamma,\\ \lim\limits_{y_2\to\infty}\boldsymbol{\nabla}_{\mathbf{y}}\psi^1(x_1,y_1,y_2) &=& 0. & \end{array}\right.$$

The condition at infinity comes from $\boldsymbol{\nabla}_{\mathbf{y}}\psi^1 = \boldsymbol{v}^0 - \boldsymbol{e}_1\dfrac{d\psi^0}{dx_1}$ and from the matching conditions combined with (13). The source term is $d\psi^0/dx_1$ and by linearity, the general solution is

$$\psi^1 = Q(\mathbf{y})\frac{d\psi^0}{dx_1} + \hat{\psi}(x_1), \tag{15}$$

with $\hat{\psi}$ any function that is in practice not necessary to determine and with the so-called cell-function Q defined by (it corresponds to take $d\psi^0/dx_1 = 1$): Q is 1-periodic with respect to y_1 and

$$\left\{\begin{array}{rcll} \Delta_{\mathbf{y}}Q &=& 0 & \text{in } \mathcal{Y},\\ \boldsymbol{\nabla}_{\mathbf{y}}Q\cdot\boldsymbol{n} &=& -\boldsymbol{e}_1\cdot\boldsymbol{n} & \text{on } \Gamma,\\ \lim\limits_{y_2\to\infty}\boldsymbol{\nabla}_{\mathbf{y}}Q(y_1,y_2) &=& 0, & \\ \lim\limits_{y_2\to\infty}Q(y_1,y_2) &=& 0. & \end{array}\right. \tag{16}$$

The condition $\lim\limits_{y_2\to\infty}Q(y_1,y_2) = 0$ has been added to define uniquely Q. In a same way Ψ^1 is given by

$$\Psi^1 = Q(\mathbf{y})\frac{d\Psi^0}{dx_1} + \hat{\Psi}(x_1), \tag{17}$$

with the same cell-function Q than already defined in (16). Note that excepting for some very particular geometries, Q cannot be determined in closed form.

Thanks to the determination of ψ^1, we can determine $\boldsymbol{v}^1$, that satisfies:

$$\left\{\begin{array}{rcll} \mathrm{div}_{\mathbf{y}}\,\boldsymbol{v}^1 + \dfrac{\partial(\boldsymbol{v}^0)_1}{\partial x_1} &=& -\psi^0 - 2iM\left(\boldsymbol{V}^0\cdot\boldsymbol{\nabla}_{\mathbf{y}}\psi^1 + (\boldsymbol{V})_1^0\dfrac{d\psi^0}{dx_1}\right) & \text{in } \mathcal{Y},\\ \boldsymbol{v}^1\cdot\boldsymbol{n} &=& 0 & \text{on } \Gamma. \end{array}\right. \tag{18}$$

To go further, we remember that $(\boldsymbol{v}^0)_1$ and $(\boldsymbol{V}^0)_1$ can be expressed versus Q. Indeed using

$$\left\{\begin{array}{rcll} \boldsymbol{v}^0 &=& \boldsymbol{\nabla}_{\mathbf{y}}\psi^1 + \boldsymbol{e}_1\dfrac{d\psi^0}{dx_1} & \text{in } \mathcal{Y},\\ \psi^1 &=& Q(\mathbf{y})\dfrac{d\psi^0}{dx_1} + \hat{\psi}(x_1) & \text{in } \mathcal{Y}, \end{array}\right.$$

leads to

$$(\boldsymbol{v}^0)_1 = \frac{d\psi^0}{dx_1}\left(\frac{\partial Q}{\partial y_1}+1\right),$$

and symmetrically we get $(\boldsymbol{V}^0)_1 = \dfrac{d\Psi^0}{dx_1}\left(\dfrac{\partial Q}{\partial y_1}+1\right)$ for the mean flow. Since $\mathrm{div}_{\mathbf{y}}\,\boldsymbol{V}^0 = 0$, the system (18) can be written in the suitable form:

$$\left\{\begin{array}{rcl} \mathrm{div}_{\mathbf{y}}(\boldsymbol{v}^1 + 2iM\boldsymbol{V}^0\psi^1) + \dfrac{d^2\psi^0}{dx_1^2}\left(\dfrac{\partial Q}{\partial y_1}+1\right) + \psi^0, & & \\ +2iM\dfrac{d\Psi^0}{dx_1}\dfrac{d\psi^0}{dx_1}\left(\dfrac{\partial Q}{\partial y_1}+1\right) & = & 0 \quad \text{in} \quad \mathcal{Y}, \\ \boldsymbol{v}^1\cdot\boldsymbol{n} & = & 0 \quad \text{on} \quad \Gamma. \end{array}\right.$$

As it has been done for $\boldsymbol{v}^0$, this equation is integrated on $\mathcal{Y}_m$ leading to

$$\begin{array}{l} \displaystyle\int_{-1/2}^{1/2}\left[(\boldsymbol{v}^1)_2(x_1,y_1,y_m) + 2iM(\boldsymbol{V}^0)_2(y_1,y_m)\,\psi^1(x_1,y_1,y_m)\right]\,dy_1 + \\ \dfrac{d^2\psi^0}{dx_1^2}\left(\displaystyle\int_{\mathcal{Y}_m}\frac{\partial Q}{\partial y_1}d\mathbf{y}\right) + \dfrac{d^2\psi^0}{dx_1^2}(y_m+S) + \psi^0(y_m+S) + \\ 2iM\dfrac{d\Psi^0}{dx_1}\dfrac{d\psi^0}{dx_1}\left(\displaystyle\int_{\mathcal{Y}_m}\frac{\partial Q}{\partial y_1}d\mathbf{y}\right) + 2iM\dfrac{d\Psi^0}{dx_1}\dfrac{d\psi^0}{dx_1}(y_m+S) = 0, \end{array} \tag{19}$$

where we have noted

$$S = \int_{\mathcal{Y}^-} d\mathbf{y}, \tag{20}$$

with $\mathcal{Y}^- = \{\mathbf{y}\in\mathcal{Y}, y_2<0\}$ (see Fig. 2), the surface inside the grooves. To deduce the boundary condition for $\boldsymbol{u}^1$, we use the matching condition at order 1 for the acoustics (see [13] for deeper details):

$$\left\{\begin{array}{rcl} \displaystyle\lim_{y_2\to\infty}\left(\psi^1(x_1,y_1,y_2) - y_2\frac{\partial\varphi^0}{\partial x_2}(x_1,0)\right) & = & \varphi^1(x_1,0), \\ \displaystyle\lim_{y_2\to\infty}\left(\boldsymbol{v}^1(x_1,y_1,y_2) - y_2\frac{\partial\boldsymbol{u}^0}{\partial x_2}(x_1,0)\right) & = & \boldsymbol{u}^1(x_1,0). \end{array}\right.$$

For $(\boldsymbol{v}^1)_2$ it read:

$$\lim_{y_m\to\infty}\left((\boldsymbol{v}^1)_2(x_1,y_1,y_m) - y_m\frac{\partial(\boldsymbol{u}^0)_2}{\partial x_2}(x_1,0)\right) = (\boldsymbol{u}^1)_2(x_1,0), \tag{21}$$

and we will show that it reads

$$\lim_{y_m\to\infty}\left[(\boldsymbol{v}^1)_2(x_1,y_1,y_m) + y_m\left(\frac{d^2\psi^0}{dx_1^2}+\psi^0+2iM\frac{d\Psi^0}{dx_1}\frac{d\psi^0}{dx_1}\right)\right] = (\boldsymbol{u}^1)_2(x_1,0). \tag{22}$$

To prove this, we only need to determine $\dfrac{\partial(\boldsymbol{u}^0)_2}{\partial x_2}(x_1,0)$. Since in the order 0 outer problem φ^0 has been found to satisfy

$$\left(\Delta_{\mathbf{x}} + 1 + 2iM\boldsymbol{U}^0\cdot\boldsymbol{\nabla}_{\mathbf{x}}\right)\varphi^0 = 0,$$

using $\boldsymbol{u}^0 = \boldsymbol{\nabla}_{\mathbf{x}}\varphi^0$ we get at all locations $(x_1, x_2) \in \Omega_\infty$

$$\frac{\partial(\boldsymbol{u}^0)_2}{\partial x_2} = \frac{\partial^2\varphi^0}{\partial x_2^2} = -\frac{\partial^2\varphi^0}{\partial x_1^2} - \varphi^0 - 2iM\boldsymbol{U}^0 \cdot \boldsymbol{\nabla}_{\mathbf{x}}\varphi^0.$$

Thus at $x_2 = 0$, since $\varphi^0(x_1, 0) = \psi^0(x_1)$, $(\boldsymbol{U}^0)_2(x_1, 0) = 0$ and $(\boldsymbol{U}^0)_1(x_1, 0) = \dfrac{d\Psi^0}{dx_1}$, we get that (21) becomes (22).

Finally using $\lim_{y_m\to\infty}(\boldsymbol{V}^0)_2(x_1, y_1, y_m) = (\boldsymbol{U}^0)_2(x_1, 0) = 0$, we get that (19) becomes

$$(\boldsymbol{u}^1)_2(x_1, 0) + \left(\frac{d^2\psi^0}{dx_1^2} + 2iM\frac{d\Psi^0}{dx_1}\frac{d\psi^0}{dx_1}\right)\left(S + \int_{\mathcal{Y}}\frac{\partial Q}{\partial y_1}d\mathbf{y}\right) + S\psi^0 = 0.$$

Noting

$$C = S + \int_{\mathcal{Y}}\frac{\partial Q}{\partial y_1}d\mathbf{y}, \tag{23}$$

and using that $\boldsymbol{u}^1 = \boldsymbol{\nabla}_{\mathbf{x}}\varphi^1$ and that $\Psi^0(x_1) = \Phi^0(x_1, 0)$, we get the boundary condition at order 1 for φ:

$$\frac{\partial\varphi^1}{\partial x_2}(x_1, 0) + C\left(\frac{\partial^2\varphi^0}{\partial x_1^2}(x_1, 0) + 2iM\frac{\partial\Phi^0}{\partial x_1}(x_1, 0)\frac{\partial\varphi^0}{\partial x_1}(x_1, 0)\right) + S\varphi^0(x_1, 0) = 0.$$

Proceeding in a same way, we get the boundary condition at order 1 for the mean flow potential Φ:

$$\frac{\partial\Phi^1}{\partial x_2}(x_1, 0) + C\frac{\partial^2\Phi^0}{\partial x_1^2}(x_1, 0) = 0.$$

Note that an alternative writing is $C = S + \int_{\mathcal{Y}^-}\partial Q/\partial y_1 d\mathbf{y}$, using for $y_2 > 0$ the periodicity of Q when integrating along y_1.

We have determined two homogenized models, one for φ^1 and another giving φ^1 versus φ^0 (the same for Φ). It is in practice much more convenient to have only one model and its derivation is done in the next paragraph.

3.3 Derivation of the unified homogenized problem

3.3.1 Model for a general flow

Let us recall that we have found, up to the order 1

$$\begin{cases} \left(\Delta_{\mathbf{x}} + 1 + 2iM\boldsymbol{\nabla}_{\mathbf{x}}\Phi^0 \cdot \boldsymbol{\nabla}_{\mathbf{x}}\right)\varphi^0 = 0, & \text{for} \quad x_2 > 0 \\ \left(\Delta_{\mathbf{x}} + 1 + 2iM\boldsymbol{\nabla}_{\mathbf{x}}\Phi^0 \cdot \boldsymbol{\nabla}_{\mathbf{x}}\right)\varphi^1 + 2iM\boldsymbol{\nabla}_{\mathbf{x}}\Phi^1 \cdot \boldsymbol{\nabla}_{\mathbf{x}}\varphi^0 = 0, & \text{for} \quad x_2 > 0 \\ \dfrac{\partial\varphi^0}{\partial x_2} = 0, & \text{at} \quad x_2 = 0, \\ \dfrac{\partial\varphi^1}{\partial x_2} + C\left(\dfrac{\partial^2\varphi^0}{\partial x_1^2} + 2iM\dfrac{\partial\Phi^0}{\partial x_1}\dfrac{\partial\varphi^0}{\partial x_1}\right) + S\varphi^0 = 0, & \text{at} \quad x_2 = 0, \end{cases}$$

for the acoustic perturbations and

$$\left\{\begin{array}{rll} \Delta_{\mathbf{x}}\Phi^0 = 0 = \Delta_{\mathbf{x}}\Phi^1, & \text{for} & x_2 > 0 \\ \dfrac{\partial\Phi^0}{\partial x_2} = 0 = \dfrac{\partial\Phi^1}{\partial x_2} + C\dfrac{\partial^2\Phi^0}{\partial x_1^2}, & \text{at} & x_2 = 0, \end{array}\right.$$

for the mean flow. Noting $\varphi^h = \varphi^0 + \varepsilon\varphi^1$ and $\Phi^h = \Phi^0 + \varepsilon\Phi^1$ the homogenized fields and combining all the equations at orders 0 and 1 is deduced the complete model in the non-dimensional $\mathbf{x}$-space at order $O(\varepsilon^2)$ (in the sense that neglected terms are of order ε^2):

$$\left\{\begin{array}{rll} \left(\Delta_{\mathbf{x}} + 1 + 2iM\boldsymbol{\nabla}_{\mathbf{x}}\Phi^h\cdot\boldsymbol{\nabla}_{\mathbf{x}}\right)\varphi^h = 0, & \text{for} & x_2 > 0 \\ \dfrac{\partial\varphi^h}{\partial x_2} + \varepsilon C\left(\dfrac{\partial^2\varphi^h}{\partial x_1^2} + 2iM\dfrac{\partial\Phi^h}{\partial x_1}\dfrac{\partial\varphi^h}{\partial x_1}\right) + \varepsilon S\varphi^h = 0, & \text{at} & x_2 = 0, \end{array}\right.$$

combined to

$$\left\{\begin{array}{rll} \Delta_{\mathbf{x}}\Phi^h = 0, & \text{for} & x_2 > 0 \\ \dfrac{\partial\Phi^h}{\partial x_2}(x_1,0) + \varepsilon C\dfrac{\partial^2\Phi^h}{\partial x_1^2}(x_1,0) = 0, & \text{at} & x_2 = 0. \end{array}\right.$$

In the actual $\mathbf{X}$-space, noting $\varphi^h(\mathbf{x}) = \varphi^h(\mathbf{X})$ with $\mathbf{x} = k\mathbf{X}$ and noting $\Phi^h(\mathbf{x}) = k\Phi^h(\mathbf{X})$, we get the complete homogenized problem (8) and (9) announced in paragraph 3.1.

For a particular far flow, the potential Φ^h can be determined in closed form as detailed now.

3.3.2 Case of an horizontal far-flow

If we consider a flow along $\boldsymbol{e}_1$ at infinity, as it will be done in the numerical illustrations, then Φ^h can be determined explicitly. Such situation corresponds to choose Φ^h such that $\lim_{X_2\to\infty}\Phi^h(\mathbf{X}) = X_1$. The solution of (9) is then very simple, it is $\Phi^h(\mathbf{X}) = X_1$ everywhere and thus (8) simplifies in

$$\left\{\begin{array}{rll} \left(\Delta_{\mathbf{X}} + k^2 + 2ikM\dfrac{\partial}{\partial X_1}\right)\varphi^h = 0, & \text{for} & X_2 > 0, \\ \dfrac{\partial\varphi^h}{\partial X_2} + hC\left(\dfrac{\partial^2\varphi^h}{\partial X_1^2} + 2ikM\dfrac{\partial\varphi^h}{\partial X_1}\right) + k^2hS\varphi^h = 0, & \text{at} & X_2 = 0. \end{array}\right. \tag{24}$$

Remark 3. *In [68] is derived a boundary condition in another configuration than ours: a flat surface is considered but the presence of a boundary shear layer along a rigid wall is taken into account, of width h small compared to the acoustic wavelength λ. The flow is characterized by its Mach profile $M_0(X_2)$ for $-h < X_2 < 0$ and is considered uniform above the boundary layer ($M_0 = M$ for $X_2 > 0$). The boundary layer localized in the area $-h < X_2 < 0$ is replaced thanks to an asymptotic analysis by an appropriate boundary condition at $X_2 = 0$, which takes into account at the second order in $\varepsilon = kh$ the effect*

of the boundary layer. For a Mach profile M_0 linear, the following boundary condition is found

$$\frac{\partial \varphi}{\partial X_2} + hD_{X_1}\left(\frac{i}{k}\frac{\partial^2}{\partial X_1^2} - D_{X_1}\right)\varphi = 0,$$

with $D_{X_1} = M\partial/\partial X_1 - ik$. Neglecting as for us the terms of order M^2, it reads

$$\frac{\partial \varphi}{\partial X_2} + h\left(\frac{\partial^2 \varphi}{\partial X_1^2} + 2ikM\frac{\partial \varphi}{\partial X_1} + k^2\varphi + i\frac{M}{k}\frac{\partial^3 \varphi}{\partial X_1^3}\right) = 0. \tag{25}$$

This condition is not the homogenized boundary condition (24) *but has some strong links with it. The condition* (25) *is exactly* (24) *if $S = 1 = C$, which could be expected since it corresponds to a flat surface at $X_2 = -h$, thus $f(y_1) = -1$, but also if the third derivative $\partial^3\varphi/\partial X_1^3$ is neglected. We have no interpretation for this last point but let us recall that we compare two very different configurations: a potential flow over a distorted surface and a rotational flow over a flat surface. Thus it is expected to find connected models but not to find exactly the same boundary condition.*

Remark 4. *We could have used Taylor's transformation [67] to transform the Low Mach model* (4) *into the simple model*

$$\left\{\begin{array}{rcl} \left(\Delta_{\mathbf{X}} + k^2\right)\xi = 0 & = & 0 \quad in \quad \Omega_\infty^{\mathbf{X}}, \\ \boldsymbol{\nabla}_{\mathbf{X}}\xi \cdot \boldsymbol{n} & = & 0 \quad on \quad \Gamma_\infty^{\mathbf{X}}. \end{array}\right. \tag{26}$$

This model seems more attractive because the acoustic is no longer coupled to the mean flow, the mean flow has even disappeared. We have not chosen this Taylor's approach for three reasons. First it does not simplify significantly the derivation of the homogenized model (for instance the same cell problem appears). Moreover the simple Helmholtz equation $\left(\Delta_{\mathbf{X}} + k^2\right)\xi = 0$ is obtained after an additional approximation which thus reduces the quality of the induced homogenized model. Indeed Taylor's transformation consists in the change of unknowns $\varphi(\mathbf{X}) = \xi(\mathbf{X})e^{-ikM\Phi(\mathbf{X})}$ with Φ the mean flow potential such that $\boldsymbol{U}(\mathbf{X}) = \boldsymbol{\nabla}_{\mathbf{X}}\Phi$ and it corresponds to the operator transformations:

$$\left\{\begin{array}{rcl} \boldsymbol{\nabla}_{\mathbf{X}} & \to & \boldsymbol{\nabla}_{\mathbf{X}} - ikM\boldsymbol{U}, \\ \Delta_{\mathbf{X}} & \to & \Delta_{\mathbf{X}} - 2ikM\boldsymbol{U}\cdot\boldsymbol{\nabla}_{\mathbf{X}} - k^2M^2|\boldsymbol{U}|^2, \end{array}\right.$$

where we remembered that the flow is potential, $\mathrm{div}_{\mathbf{X}}\,\boldsymbol{U} = 0$. Then $\Delta_{\mathbf{X}}\varphi + k^2\varphi + 2ikM\boldsymbol{U}\cdot\boldsymbol{\nabla}_{\mathbf{X}}\varphi = 0$ becomes exactly $\Delta_{\mathbf{X}}\xi + k^2(1 + M^2|\boldsymbol{U}|^2)\xi = 0$. Therefore and as announced a terms of order $O(M^2)$ has to be once again neglected to obtain the Helmholtz equation. The last reason is that since $\xi_0 + \varepsilon\xi_1 + \cdots = (\varphi_0 + \varepsilon\varphi_1 + \cdots)e^{ikM(\Phi_0 + \varepsilon\Phi_1 + \cdots)}$, the link between the old unknows φ_0, $\varphi_1 \cdots$, Φ_0, $\Phi_1 \cdots$ and the new unknowns ξ_0, $\xi_1 \cdots$ is not obvious. It is even non linear in the sense that for instance ξ_1 is not directly linked to φ_1 but depends on φ_0, φ_1, Φ_0 and Φ_1.

Remark 5. *In the time domain the homogenized model is obtained following the same process than presented before and reads for* $\varphi^h(X_1, X_2, t)$

$$\begin{cases} \left(\Delta_{\mathbf{X}} - \dfrac{1}{c_\infty^2}\dfrac{\partial^2}{\partial t^2} - \dfrac{2M}{c_\infty}\dfrac{\partial}{\partial X_1}\dfrac{\partial}{\partial t}\right)\varphi^h = 0, \\ \dfrac{\partial \varphi^h}{\partial X_2}(X_1,0,t) + hC\left(\dfrac{\partial^2\varphi^h}{\partial X_1^2}(X_1,0,t) - \dfrac{2M}{c_\infty}\dfrac{\partial^2\varphi^h}{\partial X_1 \partial t}(X_1,0,t)\right) - \dfrac{hS}{c_\infty^2}\dfrac{\partial^2\varphi^h}{\partial t^2}(X_1,0,t) = 0, \end{cases} \tag{27}$$

From these equations we can determine the acoustic energy defined above the equivalent wall chosen at $X_2 = 0$. *It is easy to derive such energy :* $dE/dt = 0$ *with* $E = E_V + E_S$ *with the volume term*

$$E_V = \frac{1}{2}\int_{\mathbb{R}\times\mathbb{R}^+}\left[\frac{1}{c_\infty^2}\left(\frac{\partial\varphi^h}{\partial t}\right)^2 + \left(\boldsymbol{\nabla}_{\mathbf{X}}\varphi^h\right)^2\right] dX_1 dX_2,$$

and with the surface term

$$E_S = \frac{h}{2}\int_{\mathbb{R}}\left[C\left(\frac{\partial\varphi^h}{\partial X_1}\right)^2(X_1,0,t) + \frac{S}{c_\infty^2}\left(\frac{\partial\varphi^h}{\partial t}\right)^2(X_1,0,t)\right] dX_1.$$

This is an energy because all the terms are positive since it is proved in [69] that $C > 0$. *For the Low Mach model* (4)*, only* E_V *exists with the same expression but with an integration over* $\Omega_\infty^{\mathbf{X}}$.

3.4 Explicit solution of the homogenized model

As for (9), explicitly solved for an horizontal far flow, the interest of the homogenized model (24) is that it is easy to solve explicitly, in particular for an incident plane wave. This will give an easy way to test the accuracy of the homogenized model.

3.4.1 Incident wave

The chosen source is an incident plane wave but the notion of a propagative plane wave in presence of a flow is not easy to define and is clarified here. We recall that we consider a mean flow satisfying $\lim_{X_2\to\infty}\boldsymbol{U}(\mathbf{X}) = \boldsymbol{e}_1$. We send from $X_2 = +\infty$ a wave with an incident angle θ: the incident wave is of the form $\varphi^{\text{inc}} = e^{i(k_1X_1 - k_2X_2)}$ with $k_1 = K\sin\theta$, $k_2 = K\cos\theta$ ($0 \le \theta < \pi/2$ and $\theta = 0$ is a wave propagating along $-\boldsymbol{e}_2$), with a wave number $K > 0$ that has to be determined. From (4) taken at $X_2 \to \infty$ (then $\boldsymbol{U} = \boldsymbol{e}_1$ and the convected Helmholtz equation $(\Delta_{\mathbf{X}} + k^2 + 2ikM\partial/\partial X_1)\varphi^{\text{inc}} = 0$ is recovered), the wave vector (k_1, k_2) is found to satisfy the dispersion relation

$$k^2 = k_1^2 + k_2^2 + 2kMk_1. \tag{28}$$

It reads also $k^2 = K^2 + 2kMK\sin\theta$ from which is deduced for a given angle θ and a given frequency k, the expression

$$K = k\left(-M\sin\theta + \sqrt{1 + (M\sin\theta)^2}\right). \tag{29}$$

3.4.2 Scattered field

For an incident plane wave, the homogenized solution $\varphi^h(\mathbf{X})$ of (24) is easy to determine explicitly: it reads

$$\varphi^h(\mathbf{X}) = e^{ik_1X_1}[e^{-ik_2X_2} + R^h e^{ik_2X_2}], \tag{30}$$

where the reflection coefficient is found to be

$$R^h = \frac{ik_2 + a}{ik_2 - a} \quad \text{where} \quad a = h[(k_1^2 + 2k_1kM)C - k^2S]. \tag{31}$$

Of course $|R^h| = 1$ since all the incident energy is reflected.

Remark 6. *For the solution $\varphi(\mathbf{X})$ of the Low Mach model (4), an expression similar to (30) can be found for the far field. Indeed we have already mentioned that (4), taken at $X_2 \to \infty$ in order to determine the far field, reduces to the convected Helmholtz equation $(\Delta_{\mathbf{X}} + k^2 + 2ikM\partial/\partial X_1)\varphi = 0$. Considering Fourier series along the direction $\boldsymbol{e}_1$, the following exact solution is found*

$$\varphi(\mathbf{X}) = e^{i(k_1X_1 - k_2X_2)} + \sum_{n=-\infty}^{\infty} R_n e^{i(k_1^{(n)}X_1 + k_2^{(n)}X_2)}, \tag{32}$$

with $k_1^{(n)} = k_1 + (2n\pi/h)$ and $k_2^{(n)} = [k^2 - (k_1^{(n)})^2 - 2kMk_1^{(n)}]^{1/2}$ with the complex square root chosen such that $\Im m(k_2^{(n)}) \geq 0$. At a low frequency k and for a low Mach number value M, only $k_2^{(0)} = k_2$ is real (we recall that $k_2 = K\cos\theta$) and thus (32) can be written in a form very similar to (30):

$$\varphi(\mathbf{X}) = e^{i(k_1X_1 - k_2X_2)} + R_0\, e^{i(k_1X_1 + k_2X_2)} + \varphi_{\text{eva}}. \tag{33}$$

Introducing $\beta_2^{(n)} = [-(k^2 - (k_1^{(n)})^2 - 2kMk_1^{(n)})]^{1/2} \geq 0$, the evanescent field is defined by $\varphi_{\text{eva}} = \sum_{n\neq 0} R_n e^{ik_1^{(n)}X_1} e^{-\beta_2^{(n)}X_2}$ and becomes negligible when $X_2 \to \infty$. In the next numerical section, R^h will be compared to R_0 (to get the far field error).

4 Numerical results

Contrary to the homogenized model (24), the Low Mach model ((4), (5)) cannot be solved in closed-form because of the curved geometry and of the variable coefficient $\boldsymbol{U}$, and it must be solved numerically. To validate numerically the accuracy of the homogenized model, the chosen numerical method depends on the complexity of the geometry and the strategy is the following: we consider first a simple geometry with rectangular grooves, for which we use the modal method developed in [70] to solve two problems, to solve (5) to determine the potential flow and to solve (4) to get the acoustic field (thanks to the help of Taylor's transformation to get rid of the variable coefficient $\boldsymbol{U}$). Then we will

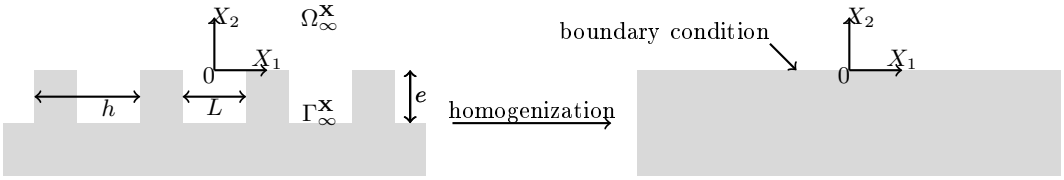

Figure 3: Geometry for rectangular grooves in dimensional $\mathbf{X}$ coordinates.

consider more involved geometries to illustrate the adaptability of the homogenized model to general geometries, requiring to use a Finite Element method to solve both the mean flow and the acoustics (then without Taylor's transformation).

For rectangular grooves of periodicity h and depth $e = O(h)$ we note L the width of the grooves ($L = 0$ corresponds to no groove, see Fig. 3). First we present how to determine the background flow Φ (which also corresponds to solve the cell problem) and then we present the determination of the acoustic field φ solution of (4).

4.1 Background flow

For an imposed velocity $\boldsymbol{e}_1$ at infinity, the mean velocity $\boldsymbol{U}(\mathbf{X}) = \boldsymbol{\nabla}_{\mathbf{X}}\Phi$ satisfies

$$\left\{\begin{array}{rcll} \Delta_{\mathbf{X}}\Phi & = & 0 & \text{in } \Omega^{\mathbf{X}}_\infty, \\ \boldsymbol{\nabla}_{\mathbf{X}}\Phi\cdot\boldsymbol{n} & = & 0 & \text{on } \Gamma^{\mathbf{X}}_\infty, \\ \lim\limits_{X_2\to\infty}\boldsymbol{\nabla}_{\mathbf{X}}\Phi & = & \boldsymbol{e}_1. & \end{array}\right. \tag{34}$$

The potential $\Phi(\mathbf{X})$ is defined up to a constant and since $\Phi(\mathbf{X}) - X_1 \to$ cst when $X_2 \to \infty$, we fix the constant to zero by imposing to Φ to tend to X_1 when X_2 tends to infinity. In practice we look for $\tilde{Q}(\mathbf{X}) = \Phi(\mathbf{X}) - X_1$, the perturbation of the uniform far field flow. Since this perturbation is induced by a h-periodic groove shape, $\tilde{Q}$ is solution in $\mathcal{Y}^{\mathbf{X}} = \{(X_1, X_2) \in \Omega^{\mathbf{X}}_\infty, X_1 \in (-h/2, h/2)\}$ of: $\tilde{Q}$ is h-periodic and satisfies

$$\left\{\begin{array}{rcll} \Delta_{\mathbf{X}}\tilde{Q} & = & 0 & \text{in } \mathcal{Y}^{\mathbf{X}}, \\ \boldsymbol{\nabla}_{\mathbf{X}}\tilde{Q}\cdot\boldsymbol{n} & = & -\boldsymbol{e}_1\cdot\boldsymbol{n} & \text{on } \Gamma^{\mathbf{X}}_\infty, \\ \lim\limits_{X_2\to\infty}\boldsymbol{\nabla}_{\mathbf{X}}\tilde{Q} & = & \mathbf{0}, & \\ \lim\limits_{X_2\to\infty}\tilde{Q} & = & 0. & \end{array}\right. \tag{35}$$

The cell problem (16) is recovered and it is straightforward to check that $\tilde{Q}(\mathbf{X}) = hQ(\mathbf{y})$ with $\boldsymbol{y} = \boldsymbol{X}/h$ (see Fig. 4) and with Q defined in (16). To sum up, $\Phi(\boldsymbol{X}) = X_1 + hQ(\boldsymbol{X}/h)$ with Q the cell function solution of (16). To visualize the flow, it is convenient to determine the stream function Ψ^f because its isovalues are the streamlines. The stream function is defined by the relation

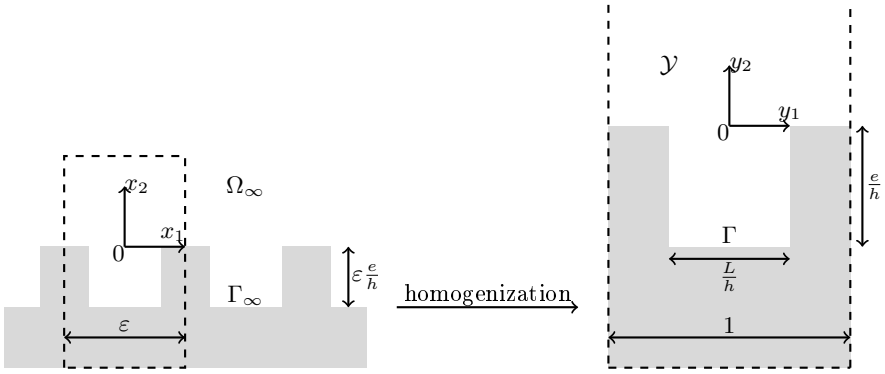

Figure 4: Cell geometry for rectangular grooves, in $\mathbf{x} = k\mathbf{X}$ and $\mathbf{y} = \mathbf{x}/\varepsilon$ coordinates.

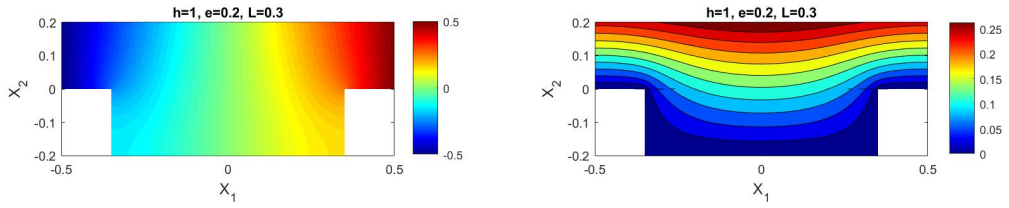

Figure 5: Mean flow; velocity potential $\Phi(\mathbf{X})$ on the left and stream function $\Psi^f(\mathbf{X})$ on the right for $h = 1$, $e = 0.2$ and $L = 0.3$

$\boldsymbol{U} = \mathbf{curl}(\Psi^f \boldsymbol{e}_3)$ and satisfies: Ψ^f is h-periodic and

$$\left\{\begin{array}{rcll} \Delta_{\mathbf{X}}\Psi^f & = & 0 & \text{in } \mathcal{Y}^{\mathbf{X}}, \\ \Psi^f & = & 0 & \text{on } \Gamma_\infty^{\mathbf{X}}, \\ \lim\limits_{X_2\to\infty} \mathbf{curl}(\Psi^f \boldsymbol{e}_3) & = & \boldsymbol{e}_1. & \end{array}\right.$$

If Φ has already been determined, by a modal method for instance as it is our case, Ψ^f can be deduced thanks to the relation $\boldsymbol{\nabla}_{\mathbf{X}}\Phi = \mathbf{curl}(\Psi^f \boldsymbol{e}_3)$, the constants of integration being adjusted by imposing $\Psi^f = 0$ on $\Gamma_\infty^{\mathbf{X}}$.

On Fig. 5 is represented in a unit cell the mean flow for a rectangular geometry (see Fig. 4): a groove of depth $e = 0.2$ and of width $L = 0.6$ for a unitary $h = 1$ periodic cell. The isovalues of the velocity potential $\Phi(\mathbf{X})$ and of the stream function $\Psi^f(\mathbf{X})$, obtained thanks to a modal method, are plotted. $\Phi(\mathbf{X})$ tends exponentially to X_1 and $\Psi^f(\mathbf{X}) - X_2$ tends exponentially to a constant when X_2 increases. The stream function $\Psi^f(\mathbf{X})$ indicates clearly how the flow is deformed by the presence of the rectangular cavity.

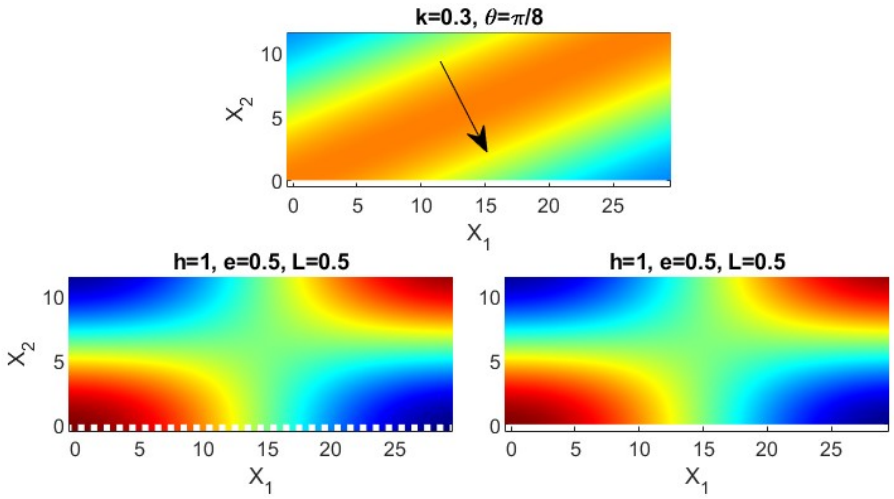

Figure 6: Real part of the acoustic velocity potentials for an incident plane wave with $k = 0.3$, $\theta = \pi/8$, $M = 0.4$, $h = 1$, $e = 0.5$ and $L = 0.5$. Top: incident field; Left: actual solution $\varphi(\mathbf{X})$; Right: homogenized solution $\varphi^h(\mathbf{X})$

4.2 Scattered field

In all the following numerical results, the geometry is fixed to $h = 1$, thus the small parameter is $\varepsilon = k$.

4.2.1 Validation of the homogenized model

On Fig. 6 are represented the real parts of the acoustic velocity potentials for an incident wave corresponding to $k = 0.3$ and a flow $M = 0.4$. The geometry is made of square cavities of size $L = 0.5 = e$. The upper figure shows the incident field with $\theta = \pi/8$. The middle figure is the actual field $\varphi(\mathbf{X})$ solution of (4) and the lower figure is the field $\varphi^h(\mathbf{X})$ solution of the homogenized model (24). It is obvious that they are very close but we can be more precise by defining two errors induced by the homogenized model: the field error defined by

$$\mathrm{E}_r^{\varphi} = \frac{\|\varphi(\mathbf{X}) - \varphi^h(\mathbf{X})\|_{L^2(\Omega)}}{\|\varphi(\mathbf{X})\|_{L^2(\Omega)}}, \tag{36}$$

where $\Omega = (-h/2, h/2) \times (0, H)$ is the comparison calculation domain (here $H = 11.5$) and it corresponds to $X_2 > 0$ since φ^h exists only for $X_2 > 0$, and the far field error

$$\mathrm{E}_r^{R} = \frac{|R_0 - R^h|}{|R_0|}, \tag{37}$$

measuring the difference between the reflection coefficient R_0 for the actual geometry and R^h for the homogenized model.

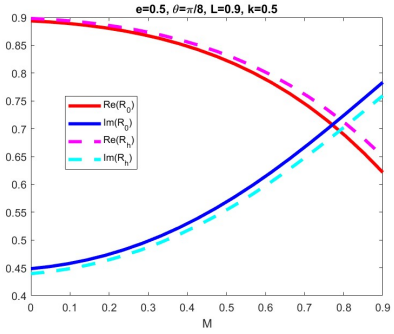

Figure 7: Real part and imaginary part of the reflection coefficients R_0 for the actual geometry and R^h for the homogenized model versus the Mach number M of the flow for an incident plane wave with $k = 0.5$, $\theta = \pi/8$, $h = 1$, $e = 0.5$ and $L = 0.9$.

The coefficient R^h is given by (31) and R_0 has been defined in (33). When using a numerical modal method, R_0 is a natural unknown of the problem and thus is directly determined. When using a Finite Element method, the unknown is $\varphi(\mathbf{X})$. Then to extract R_0, starting from (33) we introduce the scattered field

$$\varphi_S = \sum_{n=-\infty}^{\infty} R_n e^{i(k_1^{(n)} X_1 + k_2^{(n)} X_2)}, \tag{38}$$

and R_0 is obtained thanks to the relation

$$R_0 e^{ik_2 a} h = \int_0^h \varphi_S(X_1, a) e^{-ik_1 X_1} dX_1,$$

at any location $X_2 = a$ with a large enough (far enough such that $\boldsymbol{U}(X_1, a) \simeq \boldsymbol{e}_1$ is well satisfied). In Fig. 6, although $kh = 0.3$ is not very small, the errors are found small: $\mathrm{E}_r^{\varphi} = 0.021$ and $\mathrm{E}_r^{R} = 0.028$. The parameters in the homogenized model (24) are $S = (e/h)(L/h) = 0.25$ and $C = 0.042$ (C is obtained by the modal method that gave the mean flow).

4.2.2 Influence of the flow

To illustrate the flow influence on the scattering properties of a corrugated surface, on Fig. 7 are represented the real part and the imaginary part of the reflection coefficients, R_0 for the actual geometry and R^h for the homogenized model, versus the Mach number M of the mean flow. The incident plane wave corresponds to $k = 0.5$, $\theta = \pi/8$ and the surface grooves are characterized by $h = 1$, $e = 0.5$ and $L = 0.9$. Real and imaginary parts are linked since $|R^h| = 1 = |R_0|$. It appears that the reflection coefficients vary significantly when M increases. It implies that the homogenized model developed in [13] for

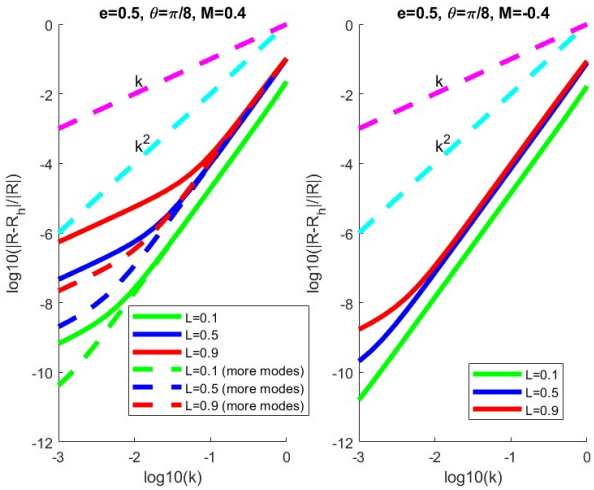

Figure 8: Reflections error $|R - R^h|/|R|$ versus k for $h = 1$, $e = 0.5$, $\theta = \pi/8$ with $L = 0.1$ (green), $L = 0.5$ (blue), $L = 0.9$ (red). Left: $M = 0.4$. Right: $M = -0.4$. The power laws k and k^2 are represented as dashed straight lines to help visualize curve slopes.

a fluid at rest $M = 0$ cannot be used for increasing Mach number values and therefore it was necessary to develop a model taking the flow into account. The error E_r^R defined in (37) goes from 0.01 to 0.04 when M goes from 0 to 0.9.

After these two illustrative examples, we present now a more quantitative study.

4.2.3 Accuracy of the homogenized model

We have determined the far field error E_r^R for varying values of several parameters, linked to the geometry, to the flow or to the incident frequency. The grooves are chosen with $e = 0.5$ and the incident angle is $\theta = \pi/8$.

Influence of L In Fig. 8 is plotted the error on the reflection coefficients E_r^φ for various L values versus the frequency k. The left figure is for $M = 0.4$ and the right figure for $M = -0.4$ ($M < 0$ corresponds to a mean flow flowing along $-\boldsymbol{e}_1$ at infinity) and three groove sizes are considered, $L = 0.1$, $L = 0.5$ and $L = 0.9$. Of course the errors decrease with $\varepsilon = kh = k$ (we recall that $h = 1$). The error is found to be lower for narrow cavities (small L values). The power laws k and k^2 are represented as dashed straight lines and it appears that for $M = -0.4$, the errors vary like k^2 as expected, up to low k values, for $k > 0.01$. The results seem to be not so good for $M = 0.4$ since the k^2 law is valid only for $k > 0.1$. For $k < 0.1$ the error surprisingly varies only like k (note however

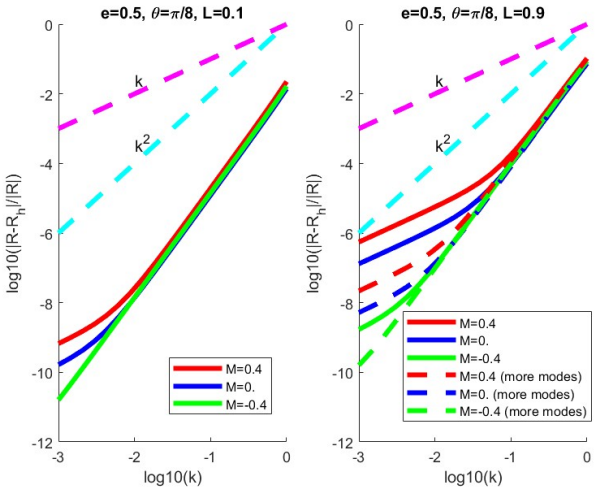

Figure 9: Reflections error $|R - R^h|/|R|$ versus k for $h = 1$, $e = 0.5$, $\theta = \pi/8$ with $M = 0.4$ (red), $M = 0.$ (blue), $M = -0.4$ (green). Left: $L = 0.1$. Right: $L = 0.9$.

that the error is very low, below 10^{-4}). This lack of decreasing is an artificial phenomenon due to the fact that the actual solution is not exact, it is calculated for a finite number of modes, which obviously is not chosen large enough for small k values. By taking ten times more modes (dashed curves), the actual solution is better calculated and the k^2 decreasing of the error is recovered for k values smaller than $k = 0.1$.

Influence of M Fig. 9 is like Fig. 8 but focusing on the influence of the mean flow velocity M: the error on the reflection coefficients E_r^φ is plotted for various M values versus the frequency k. The left figure is for narrow grooves $L = 0.1$ and the right figure for wide grooves $L = 0.9$ and three flows are considered, $M = 0.4$, $M = 0.$ and $M = -0.4$. As already seen on Fig. (8), the error is found to decrease for lower M values. For the narrow cavity $L = 0.1$, the error is found again to be lower than for $L = 0.9$. For $L = 0.9$, as in Fig. 8, the expected k^2 law for the error fails for $k < 0.1$. But once again, the k^2 law can be recovered by simply increasing the number of modes to determine a more accurate reference solution.

4.2.4 Complex geometries

To finish we present some illustrations for more complicated geometries. In these cases, a Finite Element method is preferred to a modal method and we determine both the mean flow (and thus the cell problem) and the acoustic field

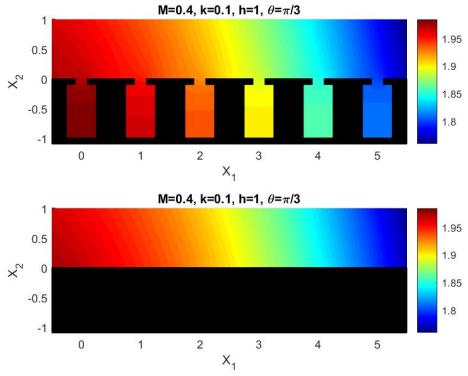

Figure 10: Real parts of the acoustic velocity potentials for a periodic cell including a Helmholtz cavity, for $k = 0.1$, $M = 0.4$ and $\theta = \pi/3$. Top: actual field $\varphi(\mathbf{X})$; Bottom: homogenized field $\varphi^h(\mathbf{X})$

thanks to the Finite Element software Xlife++ [71].

Only a periodic cell is meshed and the calculation domain is bounded by introducing a Dirichlet-to-Neumann operator on a line located in the area where the flow is no longer influenced by the lower boundary shape and thus is uniform with $\boldsymbol{U} = \boldsymbol{e}_1$. This takes place at $X_2 = a$ with a large enough. In the following results, a is taken equal to h and it has been checked to be sufficient. Still for a unit periodicity $h = 1$, the parameters of the numerical calculations are $k = 0.1$, $M = 0.4$ and $\theta = \pi/3$.

Fig. 10 and Fig. 11 represent the real parts of the acoustic velocity potentials. The upper figure is the actual solution and the lower figure the homogenized solution. Fig. 10 considers a Helmholtz cavity in each periodic cell. The neck is of width $h^- = 0.2$ and of height $d = 0.1$. The cavity extends from $X_2 = -d$ to $X_2 = -e$ with $e = 1$ and is of width $H = 0.5$. The parameters involved in the homogenized boundary condition in (24) are $S = h^- d + H(e - d) = 0.47$ and the numerical resolution of the cell problem gives $C = 0.0065$. The results are good since the errors between the actual and homogenized solutions, defined in (36) and (37), are found to be very small, $\mathrm{E}_r^{\varphi} = 0.011$ and $\mathrm{E}_r^{R} = 19.\,10^{-4}$. Note that the Helmholtz cavity is not resonating : the incident frequency $k = 0.1$ is far from the first resonance frequency noted k_r and estimated to be around $k_r \simeq \sqrt{h^-/(dS)} = 2.1$ [72]. If one wishes to take into account Helmholtz resonances, much longer cavities must be considered to get a lower resonance frequency (here to get $k_r = 0.1$ it would require $e = 400$) but then another and more involved homogenization process (in particular piecewise) must be performed as in [70, 73].

Fig. 11 consider non-symmetrical shape cavities. Fig. 11 (left) concerns a "inverse L" shape cavity and the homogenized boundary condition is characterized by $S = 0.275$ and $C = 0.0138$. The errors are found again small,

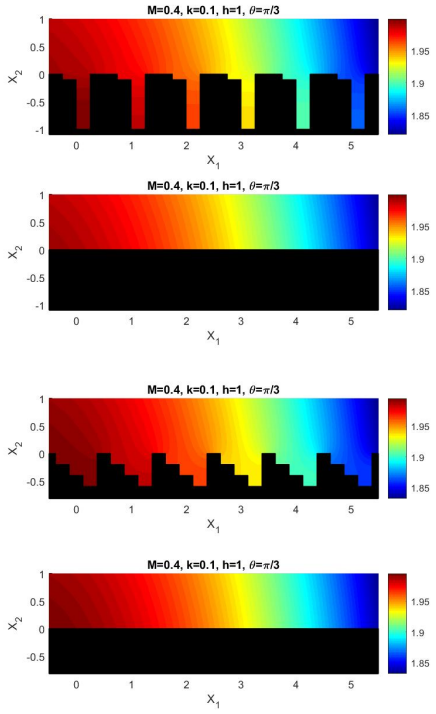

Figure 11: Real parts of the acoustic velocity potentials for for $k = 0.1$, $M = 0.4$ and $\theta = \pi/3$ and for a periodic cell including a (left): "inverse L" cavity; (right): "stair" cavity. Top: actual field $\varphi(\mathbf{X})$; Bottom: homogenized field $\varphi^h(\mathbf{X})$

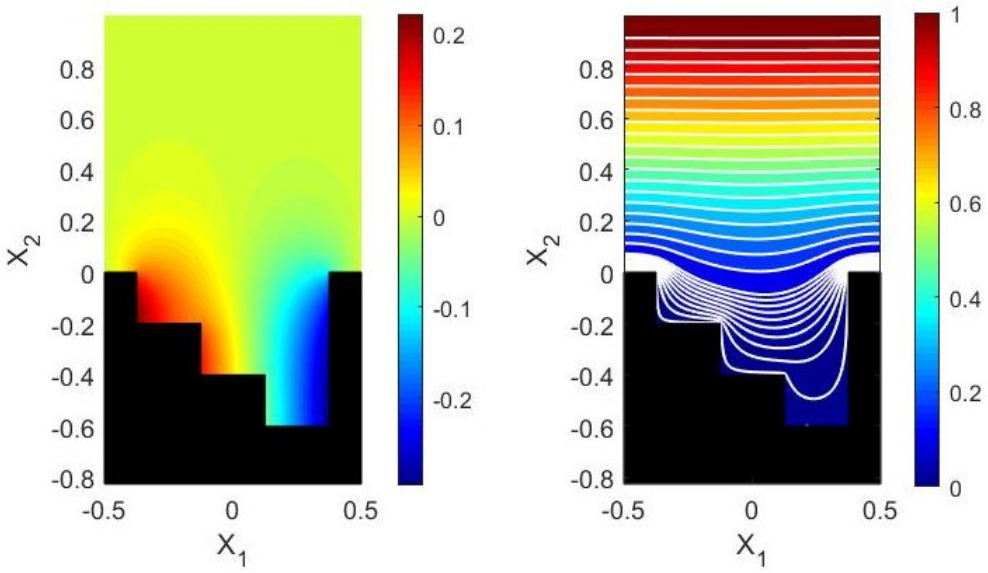

Figure 12: Mean flow in presence of a "stair" cavity. Left: perturbation of the flow potential $\tilde{Q}(\mathbf{X}) = \Phi(\mathbf{X}) - X_1$. Right: streamlines (isovalues of the stream function $\Psi^f(\mathbf{X})$);

$\mathrm{E}_r^\varphi = 7.9\,10^{-4}$ and $\mathrm{E}_r^R = 23.\,10^{-4}$. Fig. 11 (right) considers a "stair" shape cavity, the homogenized parameters are $S = 0.3$ and $C = 0.0889$ and the errors are $\mathrm{E}_r^\varphi = 0.011$ and $\mathrm{E}_r^R = 1.7\,10^{-4}$. Finally we focus closely on the mean flow to illustrate the impact of the geometry on the flow: Fig. 12 shows the mean flow velocity potential $\Phi(\mathbf{X})$ solution of (34) for the "stair" shape. To get pictures easier to read we have preferred to plot the perturbation of the potential flow, $\tilde{Q}(\mathbf{X}) = \Phi(\mathbf{X}) - X_1$ solution of (35), showing the perturbations induced by the geometry on the far field uniform flow given by $\lim_{X_2 \to \infty} \Phi(\mathbf{X}) = X_1$. Still for clarity we have also plotted the streamlines, showing the flow filling the "stair" cavity.

5 Conclusion

In this paper, we have presented a surface homogenization for acoustic waves in presence of a slow 2D potential flow in the frequency domain. We derived a surface model to characterize the effective behavior of a thin structured hard wall. The characteristic parameters of the surface are given solving an elementary potential flow problem. The model has been numerically validated and its accuracy has been measured. A natural extension is to take into account the next order of the Mach number, namely the terms proportional to M^2. This is

not simple, especially for the mean flow for which compressibility can no longer be neglected and which therefore satisfies a nonlinear equation, not easy to solve even by asymptotic expansions. On the contrary the extension to a 3D geometry would be simple to realize theoretically, but the numeric calculations are then much more difficult to realize and less easy to visualize and interpret.

A natural question that has not been addressed in this paper is the relevance of a potential flow model in the vicinity of a rough, wavy surface. To answer to this question, alternative models taking into account the vorticity of the mean flow and of the acoustic perturbations should be considered, notably models including the viscosity like the compressible Navier-Stokes equations. Of course the direct consequence is that the calculations for the establishment of a homogenized model are much more difficult. Note that in remark 3 two homogenized models obtained starting from very different flows, a non potential flow (a shear flow) or a potential flow, are compared and it appears that they give similar boundary conditions. It seems thus that when a boundary layer becomes very thin, to consider a curl-free or a not curl-free flow does not deeply change the asymptotic boundary condition.

A Derivation of the potential wave equation

In this appendix we recall how to derive the potential wave equation. It is done in [55] but here it is presented differently and with more details.

A.1 Case of a barotropic flow

We consider a barotropic flow: the pressure p only depends on the density $\hat{\rho}$, $p = f(\hat{\rho})$. The sound velocity is defined by $\hat{c}^2 = dp/d\hat{\rho} = f'(\hat{\rho})$, and the specific enthalpy $h(\hat{\rho})$ is defined by

$$\frac{dh}{d\hat{\rho}} = \frac{1}{\hat{\rho}}\frac{dp}{d\hat{\rho}} = \frac{\hat{c}^2(\hat{\rho})}{\hat{\rho}}.$$

We consider a potential flow $\boldsymbol{U} = \boldsymbol{\nabla}_{\mathbf{X}}\Phi$, tending to a uniform velocity $\boldsymbol{U}_\infty/U_\infty$ at infinity. The Bernoulli relation and the mass conservation read [61]

$$\left\{\begin{array}{rcl} \dfrac{\partial\Phi}{\partial t} + \dfrac{|\boldsymbol{U}|^2}{2} + h & = & a \in \mathbb{R}, \\ \dfrac{\partial\hat{\rho}}{\partial t} + \mathrm{div}_{\mathbf{X}}(\hat{\rho}\boldsymbol{U}) & = & 0, \\ \lim_{X_2\to\infty} \boldsymbol{U} & = & \boldsymbol{U}_\infty/U_\infty. \end{array}\right.$$

Now we introduce asymptotic expansions of the unknowns with respect to a small parameter η corresponding to the amplitude of the acoustic perturbations (due in general to a source of known small strength η, source not specified here):

$$\Phi = \Phi_0+\eta\Phi_1+\eta^2\Phi_2+\cdots, \quad \boldsymbol{U} = \boldsymbol{U}_0+\eta\boldsymbol{U}_1+\eta^2\boldsymbol{U}_2+\cdots, \quad \hat{\rho} = \hat{\rho}_0+\eta\hat{\rho}_1+\eta^2\hat{\rho}_2+\cdots$$

The order 0 is the mean flow $(\Phi_0, \boldsymbol{U}_0)$ chosen stationary and it satisfies:

$$\left\{\begin{array}{rcl} \boldsymbol{U}_0 &=& \boldsymbol{\nabla}_{\mathbf{X}}\Phi_0, \\ \dfrac{|\boldsymbol{U}_0|^2}{2} + h(\hat{\rho}_0) &=& \dfrac{U_\infty^2}{2} + h_\infty, \\ \mathrm{div}_{\mathbf{X}}(\hat{\rho}_0\boldsymbol{U}_0) &=& 0, \\ \lim_{X_2\to\infty} \boldsymbol{U}_0 &=& \boldsymbol{U}_\infty/U_\infty, \end{array}\right.$$

with $U_\infty = |\boldsymbol{U}_\infty|$. Therefore $\hat{\rho}_0 = g(|\boldsymbol{U}_0|)$ with the function

$$g(x) = h^{-1}\left(h_\infty + \frac{U_\infty^2 - x^2}{2}\right),$$

and the mean flow is solution of the non-linear equation $\mathrm{div}_{\mathbf{X}}[g(|\boldsymbol{U}_0|)\boldsymbol{U}_0] = 0$. At order 1, using

$$h(\hat{\rho}_0 + \eta\hat{\rho}_1 + \cdots) = h_0 + \eta\hat{\rho}_1 h'(\hat{\rho}_0) + \cdots = h_0 + \eta\hat{\rho}_1\frac{\hat{c}^2(\hat{\rho}_0)}{\hat{\rho}_0} + \cdots,$$

we get that Φ_1 satisfies

$$\left\{\begin{array}{rcl} \boldsymbol{U}_1 &=& \boldsymbol{\nabla}_{\mathbf{X}}\Phi_1, \\ \dfrac{\partial\Phi_1}{\partial t} + \boldsymbol{U}_0\cdot\boldsymbol{U}_1 + \dfrac{\hat{\rho}_1}{\hat{\rho}_0}\hat{c}_0^2 &=& 0, \\ \dfrac{\partial\hat{\rho}_1}{\partial t} + \mathrm{div}_{\mathbf{X}}(\hat{\rho}_1\boldsymbol{U}_0) + \mathrm{div}_{\mathbf{X}}(\hat{\rho}_0\boldsymbol{U}_1) &=& 0, \end{array}\right.$$

with $\hat{c}_0^2 = f'(\hat{\rho}_0)$. Using $\mathrm{div}_{\mathbf{X}}(\hat{\rho}_0\boldsymbol{U}_0) = 0$, the previous system can be written

$$\left\{\begin{array}{rcl} \dfrac{\partial\Phi_1}{\partial t} + \boldsymbol{U}_0\cdot\boldsymbol{\nabla}_{\mathbf{X}}\Phi_1 + \dfrac{\hat{\rho}_1}{\hat{\rho}_0}\hat{c}_0^2 &=& 0, \\ \hat{\rho}_0\dfrac{\partial}{\partial t}\left(\dfrac{\hat{\rho}_1}{\hat{\rho}_0}\right) + (\hat{\rho}_0\boldsymbol{U}_0\cdot\boldsymbol{\nabla}_{\mathbf{X}})\left(\dfrac{\hat{\rho}_1}{\hat{\rho}_0}\right) + \mathrm{div}_{\mathbf{X}}(\hat{\rho}_0\boldsymbol{\nabla}_{\mathbf{X}}\Phi_1) &=& 0. \end{array}\right.$$

Introducing the convective operator $\hat{D}_{\mathbf{X}} = \partial/\partial t + \boldsymbol{U}_0\cdot\boldsymbol{\nabla}_{\mathbf{X}}$, it gives the potential wave equation in a 2D propagation domain $\Omega_\infty^{\mathbf{X}}$

$$\left\{\begin{array}{rcl} \dfrac{\hat{\rho}_1}{\hat{\rho}_0} &=& -\dfrac{1}{\hat{c}_0^2}\hat{D}_{\mathbf{X}}\Phi_1, \\ \hat{\rho}_0\hat{D}_{\mathbf{X}}\left(\dfrac{1}{\hat{c}_0^2}\hat{D}_{\mathbf{X}}\Phi_1\right) &=& \mathrm{div}_{\mathbf{X}}(\hat{\rho}_0\boldsymbol{\nabla}_{\mathbf{X}}\Phi_1), \end{array}\right.$$

with the mean flow satisfying

$$\left\{\begin{array}{rcll} \mathrm{div}_{\mathbf{X}}\,(\hat{\rho}_0\boldsymbol{U}_0) &=& 0 & \text{in } \Omega_\infty^{\mathbf{X}}, \\ \boldsymbol{U}_0 &=& \boldsymbol{\nabla}_{\mathbf{X}}\Phi_0 & \text{in } \Omega_\infty^{\mathbf{X}}, \\ \boldsymbol{U}_0\cdot\boldsymbol{n} &=& 0 & \text{on } \Gamma_\infty^{\mathbf{X}}, \\ \lim_{X_2\to\infty}\boldsymbol{U}_0 &=& \boldsymbol{U}_\infty. & \end{array}\right.$$

To clarify the simplifications when considering the Low Mach regime, we need to determine explicitly h^{-1}. In this aim, we consider adiabatic transformations leading to an explicit expression of the state low $f(\hat{\rho})$.

A.2 Case of an adiabatic flow

For an adiabatic flow, $p = \alpha\hat{\rho}^\gamma$ with γ the adiabatic index, leading to $\hat{c}^2 = \alpha\gamma\hat{\rho}^{\gamma-1}$ and

$$h(\hat{\rho}) = \alpha\frac{\gamma}{\gamma-1}\hat{\rho}^{\gamma-1} = \frac{\hat{c}^2}{\gamma-1}.$$

Using the notations of the body of the paper, $(\Phi^0, \boldsymbol{U}^0)$ is now noted $(\Phi, U_\infty\boldsymbol{U})$, Φ^1 is noted φ and thus the acoustic perturbations satisfy the potential wave equation

$$\left\{\begin{array}{rcll} \hat{\rho}_0\hat{\mathrm{D}}_{\mathbf{X}}\left(\dfrac{1}{\hat{c}_0^2}\hat{\mathrm{D}}_{\mathbf{X}}\varphi\right) & = & \mathrm{div}_{\mathbf{X}}\left(\hat{\rho}_0\boldsymbol{\nabla}_{\mathbf{X}}\varphi\right) & \text{in } \Omega_\infty^{\mathbf{X}}, \\ \boldsymbol{\nabla}_{\mathbf{X}}\varphi\cdot\boldsymbol{n} & = & 0 & \text{on } \Gamma_\infty^{\mathbf{X}}, \end{array}\right.$$

with the mean flow satisfying

$$\left\{\begin{array}{rcll} \mathrm{div}_{\mathbf{X}}\left(\hat{\rho}_0\boldsymbol{U}\right) & = & 0 & \text{in } \Omega_\infty^{\mathbf{X}}, \\ \boldsymbol{U} & = & \boldsymbol{\nabla}_{\mathbf{X}}\Phi & \text{in } \Omega_\infty^{\mathbf{X}}, \\ \boldsymbol{U}\cdot\boldsymbol{n} & = & 0 & \text{on } \Gamma_\infty^{\mathbf{X}}, \\ \lim_{X_2\to\infty}\boldsymbol{U} & = & \boldsymbol{U}_\infty/U_\infty, & \end{array}\right.$$

where the convective operator became $\hat{\mathrm{D}}_{\mathbf{X}} = \partial/\partial t + U_\infty\boldsymbol{U}\cdot\boldsymbol{\nabla}_{\mathbf{X}}$. Then the Bernoulli relation simplifies in

$$\frac{\hat{c}_0^2}{\gamma-1} + \frac{|U_\infty\boldsymbol{U}|^2}{2} = \frac{c_\infty^2}{\gamma-1} + \frac{|U_\infty|^2}{2}, \tag{39}$$

with c_∞ the sound speed at infinity, linking the sound velocity $\hat{c}_0$ to $\boldsymbol{U}$:

$$\hat{c}_0^2 = c_\infty^2 + \frac{\gamma-1}{2}|U_\infty|^2(1-|\boldsymbol{U}|^2).$$

The density $\hat{\rho}_0$ versus $\boldsymbol{U}$ is deduced thanks to the state law $\hat{c}_0^2 = \alpha\gamma\hat{\rho}_0^{\gamma-1}$. A main difficulty is that the equation for $\boldsymbol{U}$ is non-linear since $\hat{\rho}_0$ depends on $\boldsymbol{U}$.

A.3 Dimensionless equations

We consider the time harmonic regime of frequency ω ($e^{-i\omega t}$). In dimensionless form, introducing the wave number $k = \omega/c_\infty$, the density ρ_∞ at infinity, the dimensionless density $\rho_0(\mathbf{X}) = \hat{\rho}_0/\rho_\infty$ and the dimensionless sound speed $c_0(\mathbf{X}) = \hat{c}_0/c_\infty$, we get the coupled system for $(\varphi, \boldsymbol{U}, \Phi)$:

$$\left\{\begin{array}{rcll} \rho_0\mathrm{D}_{\mathbf{X}}\left(\dfrac{1}{c_0^2}\mathrm{D}_{\mathbf{X}}\varphi\right) & = & \mathrm{div}_{\mathbf{X}}(\rho_0\boldsymbol{\nabla}_{\mathbf{X}}\varphi) & \text{in } \Omega_\infty^{\mathbf{X}}, \\ \boldsymbol{\nabla}_{\mathbf{X}}\varphi\cdot\boldsymbol{n} & = & 0 & \text{on } \Gamma_\infty^{\mathbf{X}}, \\ \mathrm{div}_{\mathbf{X}}\left(\rho_0\boldsymbol{U}\right) & = & 0 & \text{in } \Omega_\infty^{\mathbf{X}}, \\ \boldsymbol{U} & = & \boldsymbol{\nabla}_{\mathbf{X}}\Phi & \text{in } \Omega_\infty^{\mathbf{X}}, \\ \boldsymbol{U}\cdot\boldsymbol{n} & = & 0 & \text{on } \Gamma_\infty^{\mathbf{X}}, \end{array}\right. \tag{40}$$

where $\mathrm{D}_{\mathbf{X}} = M\boldsymbol{U}\cdot\boldsymbol{\nabla}_{\mathbf{X}} - ik$, with $M = U_\infty/c_\infty$ the Mach number at infinity and Bernoulli relation(39) and the state law becomes

$$c_0^2 = 1 + \frac{\gamma-1}{2}M^2(1-|\boldsymbol{U}|^2) = \rho_0^{\gamma-1}. \tag{41}$$

B Simplifications for a low Mach number flow

When the mean flow is associated to a low Mach number, the potential wave equation can be deeply simplified. Indeed, when neglecting the terms of order M^2, at order M (41) gives $c_0 \simeq 1$ and $\rho_0 \simeq 1$ and the potential wave equation eq. (40) becomes the Taylor wave equation as named in [55]:

$$\left\{\begin{array}{rcl} \Delta_{\mathbf{X}}\varphi + k^2\varphi + 2ikM\boldsymbol{U}\cdot\boldsymbol{\nabla}_{\mathbf{X}}\varphi = 0 & = & 0 \quad \text{in} \quad \Omega_\infty^{\mathbf{X}}, \\ \boldsymbol{\nabla}_{\mathbf{X}}\varphi\cdot\boldsymbol{n} & = & 0 \quad \text{on} \quad \Gamma_\infty^{\mathbf{X}}, \end{array}\right.$$

whereas the mean flow satisfies the linear equation

$$\left\{\begin{array}{rcll} \mathrm{div}_{\mathbf{X}}\,\boldsymbol{U} & = & 0 & \text{in} \quad \Omega_\infty^{\mathbf{X}}, \\ \boldsymbol{U} & = & \boldsymbol{\nabla}_{\mathbf{X}}\Phi & \text{in} \quad \Omega_\infty^{\mathbf{X}}, \\ \boldsymbol{U}\cdot\boldsymbol{n} & = & 0 & \text{on} \quad \Gamma_\infty^{\mathbf{X}}. \end{array}\right.$$

Note that in particular the mean flow no longer satisfies the non-linear equation $\mathrm{div}_{\mathbf{X}}\,[\rho_0(\boldsymbol{U})\boldsymbol{U}] = 0$ thanks to the Low Mach approximation. On the other side the acoustic φ keeps on being coupled to the mean flow $\boldsymbol{U}$, even after the Low Mach approximation.

References

[1] Lahiri C, Sadig S, Gerendas M, Enghardt L, Bake F., Establishment of a high quality database for the modelling of perforated liners, *J. Eng. Gas Turbines Power* **133**, 091503 (2011) (doi:10.1115/1.4002891)

[2] Busse-Gerstengarbe S, Nitsch S, Bake F, Enghardt L., Study on a generic nonlocally reacting liner, *AIAA J.* **53**, J053021 (2014 (doi:10.2514/1.J053021)

[3] L. Schwan, A. Geslain, V. Romero-Garcia, and J. P. Groby, Complex dispersion relation of surface acoustic waves at a lossy metasurface, *Appl. Phys. Lett.* **110**, 051902 (2017).

[4] Mellish, S., Taherzadeh, S., and Attenborough, K., Approximate impedance models for point-to-point sound propagation over acoustically-hard ground containing rectangular grooves, *The Journal of the Acoustical Society of America* **147**(1), 74-84 (2020).

[5] I. Bashir, S. Taherzadeh, and K. Attenborough, urface waves over periodically spaced strips, *J. Acoust. Soc. Am.* **134**, 4691-4697 (2013).

[6] S. Taherzadeh, I. Bashir, T. Hill, K. Attenborough, and M. Hornikx, Reduction of surface transport noise by ground roughness, *Appl. Acoust.* **83**, 1-15 (2014).

[7] I. Bashir, S. Taherzadeh, and K. Attenborough, Diffraction-assisted rough ground effect: Models and data, *J. Acoust. Soc. Am.* **133**, 1281-1292 (2013).

[8] M. S. Tong, L. Y. Ting, W. C. Chew, and M. J. White, A study for sound wave scattering by corrugated ground with complex trench structures, *Waves Random Complex Media* **19**, 392-408 (2009).

[9] L. Kelders, J. F. Allard, and W. Lauriks, Ultrasonic surface waves above rectangular-groove gratings, *J. Acoust. Soc. Am.* **103**(5), 2730-2733 (1998).

[10] Ward, G. P., Hibbins, A. P., Sambles, J. R., and Smith, J. D., Acoustic transmission through compound subwavelength slit arrays, *Physical Review B* **94**(2) (2016): 024304.

[11] Schnitzer, O., Spoof surface plasmons guided by narrow grooves, *Physical Review B* **96**(8) (2017): 085424.

[12] Cselyuszka, N., Alù, A., and Janković, N., Spoof-fluid-spoof acoustic waveguide and its applications for sound manipulation, *Physical Review Applied* **12**(5) (2019): 054014.

[13] Marigo, J. J., and Maurel, A., Homogenization models for thin rigid structured surfaces and films, *The Journal of the Acoustical Society of America* **140**(1), 260-273 (2016).

[14] A. S. Bonnet-Bendhia, D. Drissi, and N. Gmati, Simulation of muffler's transmission losses by a homogenized finite element method, *J. Comp. Acoust.* **12**, 447-474 (2004).

[15] B. Delourme, H. Haddar, and P. Joly, Approximate models for wave propagation across thin periodic interfaces, *J. Math. Pures Appl.* **98**, 28-71 (2012).

[16] Claeys X, Delourme B., High order asymptotics for wave propagation across thin periodic interfaces, *Asymptotic Anal.* **83**, 35-82 (2013) (doi:10.3233/ASY-2012-1150)

[17] Semin, A., and Schmidt, K., On the homogenization of the acoustic wave propagation in perforated ducts of finite length for an inviscid and a viscous model, *Proceedings of the Royal Society A: Mathematical, Physical and Engineering Sciences* **474**(2210), 20170708 (2018).

[18] Y. Capdeville and J.-J. Marigo, Second order homogenization of the elastic wave equation for non-periodic layered media, *Geophys. J. Int.* **170**, 823-838 (2007).

[19] Haddar H, Joly P, Nguyen HM., Generalized impedance boundary conditions for scattering by strongly absorbing obstacles: the scalar case, *Math. Models Methods Appl. Sci.* **15**, 1273-1300 (2005) (doi:10.1142/S021820250500073X)

[20] J.-R. Poirier, A. Bendali, and P. Borderies, Impedance boundary conditions for the scattering of time-harmonic waves by rapidly varying surfaces, *IEEE Trans. Antennas and Propagation* **54**, 995-1005 (2006).

[21] Holloway, C. L., Kuester, E. F., Gordon, J. A., O'Hara, J., Booth, J., and Smith, D. R., An overview of the theory and applications of metasurfaces: The two-dimensional equivalents of metamaterials, *IEEE antennas and propagation magazine* **54.2**, 10-35 (2012).

[22] Delourme, B., Haddar, H., and Joly, P., On the well-posedness, stability and accuracy of an asymptotic model for thin periodic interfaces in electromagnetic scattering problems, *Mathematical Models and Methods in Applied Sciences* **23**(13), 2433-2464 (2013).

[23] P. Mungur, H. E. Plumblee, Propagation and Attenuation of Sound in a Soft-walled Annular Duct containing a Sheared Flow, NASA SP-207, 305-327 (1969).

[24] Lazeroms, W. M. J., Sound propagation in slowly varying lined ducts with temperature gradients, Diss. Master Thesis, Eindhoven University of Technology (2010).

[25] Gabard, G., and Brambley, E. J., A full discrete dispersion analysis of time-domain simulations of acoustic liners with flow, *Journal of Computational Physics* **273**, 310-326 (2014).

[26] S.W. Rienstra., Impedance models in time domain, including the extended Helmholtz resonator model, in 12th AIAA/CEAS Aeroacoustics Conference, Cambridge, MA, USA, AIAA paper 2006-2686 (2006).

[27] Gabard, G., A comparison of impedance boundary conditions for flow acoustics, *Journal of Sound and Vibration* **332**(4), 714-724 (2013).

[28] E.J. Brambley, Review of acoustic liner models with flow, in Société Française d'Acoustique, editor, Acoustics 2012 Nantes, pages 3429–3434, Nantes, France (2012).

[29] M.K. Myers, On the acoustic boundary condition in the presence of flow, *Journal of Sound and Vibration* **71**(3), 429-434 (1980).

[30] K.U. Ingard, Influence of fluid motion past a plane boundary on sound reflection, absorption and transmission, *Journal of the Acoustical Society of America* **31**(7), 1035-1036 (1959).

[31] E. Rohan, R. Cimrman, Modelling wave dispersion in fluid saturating periodic scaffolds, *Applied Mathematics and Computation* **410** 126256 (2021), doi:https://doi.org/10.1016/j.amc.2021.126256.

[32] E. Rohan, V. Lukes, Homogenization of the vibro-acoustic transmission on periodically perforated elastic plates interacting with flow (November 2022), DOI: 10.48550/arXiv.2211.06199 https://arxiv.org/abs/2211.06199

[33] E. Rohan, V. Lukes, Homogenization of the acoustic transmission through perforated layer, *J. Comput. Appl. Math.* **234** 1876-1885 (2010), doi:10.1016/j.cam.2009.08.059.

[34] E. Rohan, V. Lukes, Homogenization of the vibro-acoustic transmission on perforated plates, *Appl. Math. Comput.* **361**821-845 (2019), doi:10.1016/j.amc.2019.06.005.

[35] Beavers, G. S., and Joseph, D. D., Boundary conditions at a naturally permeable wall, *Journal of fluid mechanics* **30**(1), 197-207 (1967).

[36] Barrenechea, G. R., Le Tallec, P., and Valentin, F., New wall laws for the unsteady incompressible Navier-Stokes equations on rough domains, *ESAIM: Mathematical Modelling and Numerical Analysis* **36**(2), 177-203 (2002).

[37] Bresch, D., Desjardins, B., Grenier, E., and Lin, C. K., Low Mach number limit of viscous polytropic flows: formal asymptotics in the periodic case, *Studies in Applied Mathematics* **109**(2), 125-149 (2002).

[38] Amirat, Y., Bodart, O., De Maio, U., and Gaudiello, A., Asymptotic approximation of the solution of the Laplace equation in a domain with highly oscillating boundary, *SIAM journal on mathematical analysis* **35**(6), 1598-1616 (2004).

[39] Mikelic, A., Rough boundaries and wall laws. Qualitative properties of solutions to partial differential equations, *Lecture Notes of Necas Center for Mathematical Modeling*, edited by E. Feireisl, P. Kaplicky and J. Malek, **5**, 103-134 (2009).

[40] Gérard-Varet, D., and Masmoudi, N., Relevance of the slip condition for fluid flows near an irregular boundary, *Communications in Mathematical Physics* **295**(1), 99-137 (2010).

[41] Dalibard, A. L., and Gérard-Varet, D., Effective boundary condition at a rough surface starting from a slip condition, *Journal of Differential Equations* **251**(12), 3450-3487 (2011).

[42] Scaraggi, M., Carbone, G., Persson, B. N., and Dini, D., Lubrication in soft rough contacts: A novel homogenized approach. Part I-Theory, *Soft Matter* **7**(21), 10395-10406 (2011).

[43] de Boer, G., and Almqvist, A., On the two-scale modelling of elastohydrodynamic lubrication in tilted-pad bearings, *Lubricants* **6**(3), 78 (2018).

[44] Almqvist, A., Fabricius, J., and Wall, P., Homogenization of a Reynolds equation describing compressible flow, *Journal of Mathematical Analysis and Applications* **390**(2), 456-471 (2012).

[45] Schwendeman, D. W., Please, C. P., Tilley, B. S., and Hendriks, F., A homogenization analysis of the compressible flow between a slider and a moving patterned rough surface, *IMA Journal of Applied Mathematics* **80**(1), 177-211 (2015).

[46] Deolmi, G., Dahmen, W., and Müller, S., Effective boundary conditions: a general strategy and application to compressible flows over rough boundaries. *Communications in Computational Physics* **21**(2), 358-400 (2017).

[47] H. Galbrun, Propagation d'une onde sonore dans l'atmosphère terrestre et théorie des zones de silence, Gauthier-Villars, Paris, France (1931).

[48] A. S. Bonnet-Ben Dhia, E. M. Duclairoir and J. F. Mercier, Acoustic propagation in a flow: numerical simulation of the time-harmonic regime, *ESAIM Proceedings* **22** (2007).

[49] W. A. Möhring, A well proposed acoustic analogy based on a moving acoustic medium, *Proceedings 1st Aeroacoustic Workshop* (in connection with the german research project SWING), Dresden (1999).

[50] C. Legendre, G. Lielens, J.-P. Coyette, Sound Propagation in a sheared flow based on fluctuating total enthalpy as generalized acoustic variable, *Proceedings of of the Internoise 2012/ASME NCAD meeting*, New York City, NY, USA (2012).

[51] M. E. Goldstein, Unsteady vortical and entropic distortion of potential flows round arbitrary obstacles, *J. Fluid Mech.* **89**(3), 433-468 (1978).

[52] D. Blokhintzev, The propagation of sound in an inhomogeneous and moving medium I., *J. Acoust. Soc. Am.* **18**(2), 322-328 (1946).

[53] A. D. Pierce, Wave equation for sound in fluids with unsteady inhomogeneous flow, *J. Acoust. Soc. Am.* **87**(6), 2292-2299 (1990).

[54] R.J. Astley, A Finite element, wave envelope formulation for acoustical radiation inmoving flows, *J. Sound and Vib.* **103**, 471-485 (1985).

[55] S. Mancini, R. J. Astley, S. Sinayoko, G. Gabard and M. Tournour, An integral formulation for wave propagation on weakly non-uniform potential flows, *Journal of Sound and Vibration* **385**, 184-201 (2016).

[56] N. Balin, F. Casenave, F. Dubois, E. Duceau, S. Duprey and I. Terrasse, Boundary element and Finite element coupling for aeroacoustics simulations, physics.comp-hp, arXiv:1402.2439, 1-23 (2014).

[57] C.J. Chapman, Similarity variables for sound radiation in a uniform flow, *J. Sound and Vib.*, **233**, 157-164 (2000).

[58] A. Gregory, S. Sinayoko, A. Agarwal and J. Lasenby, An acoustic space-time and the Lorentz transformation in aeroacoustics, physics. u-dyn, arXiv:1403.7511, 1-28 (2014).

[59] A. Agarwal and A.P. Dowling, Low frequency acoustic shielding by the silent aircraft airframe, *AIAA J.* **45**, 358-365 (2007).

[60] R.J. Astley and J.G. Bain, A 3D boundary element scheme for acoustic radiation in low Mach number, *J. Sound and Vib.* **109**, 445-465 (1986).

[61] S. Mayoral and D. Papamoschou, Prediction of jet noise shielding with forward flight effects, 51st AIAA Aerosp. Meet. (Grapevin, Texas), AIAA 2013-0010 (2013).

[62] Pagneux, V., and Froelich, B., Influence of low Mach number shear flow on acoustic propagation in ducts, *Journal of Sound and vibration* **246**(1), 137-155 (2001).

[63] Munz, C. D., Dumbser, M., and Roller, S., Linearized acoustic perturbation equations for low Mach number flow with variable density and temperature, *Journal of Computational Physics* **224**(1), 352-364 (2007).

[64] Clancy, C., and Rice, H., Acoustic shielding in low mach number potential flow incorporating a wake model using BEM, *15th AIAA/CEAS Aeroacoustics Conference* (30th AIAA Aeroacoustics Conference) (2009).

[65] Khalighi, Y., Mani, A., Ham, F., and Moin, P., Prediction of sound generated by complex flows at low Mach numbers, *AIAA journal* **48**(2), 306-316 (2010).

[66] Nana, C., Marx, D., Prax, C., and Fortuné, V., The perturbed low Mach number approximation for the aeroacoustic computation of anisothermal flows, *Acoustics 2012* (2012).

[67] K. Taylor, A transformation of the acoustic equation with implications for wind-tunnel and low-speed flight tests, *Proc. R. Soc. London* **65**, 125-136 (1979).

[68] Bonnet-Ben Dhia, A. S., Joly, P., and Joubert, L., Asymptotic modeling of boundary layers in aeroacoustics, 17th AIAA/CEAS Aeroacoustics Conference (32nd AIAA Aeroacoustics Conference), Portland, Oregon (2011).

[69] Marigo, J. J., Maurel, A., Pham, K., and Sbitti, A., Effective dynamic properties of a row of elastic inclusions: the case of scalar shear waves, *Journal of elasticity* **128**(2), 265-289 (2017).

[70] Maurel, A., Mercier, J. F., Pham, K., Marigo, J. J., and Ourir, A. Enhanced resonance of sparse arrays of Helmholtz resonators-Application to perfect absorption, *The Journal of the Acoustical Society of America*, **145**(4), 2552-2560 (2019).

[71] `https://uma.ensta-paris.fr/soft/XLiFE++/`

[72] Mercier, J. F., Marigo, J. J., and Maurel, A., Influence of the neck shape for Helmholtz resonators, *The Journal of the Acoustical Society of America* **142**(6), 3703-3714 (2017).

[73] Maurel, A., Marigo, J. J., Mercier, J. F., and Pham, K., Modelling resonant arrays of the Helmholtz type in the time domain, *Proceedings of the Royal Society A: Mathematical, Physical and Engineering Sciences* **474**(2210) 20170894 (2018).

[74] Xiwen, D. and Aurégan Y., A cavity-by-cavity description of the aeroacoustic instability over a liner with a grazing flow, *Journal of Fluid Mechanics* **852**, 126-145 (2018).